CHARACTERISATION AND BENEFICIATION STUDIES OF KUDREMUKH IRON ORE TAILING

A Thesis Submitted
In Partial Fulfilment of the Requirements
for the Degree of

MASTER OF TECHNOLOGY

by

S. A. RAVISANKAR

to the

DEPARTMENT OF METALLURGICAL ENGINEERING
INDIAN INSTITUTE OF TECHNOLOGY, KANPUR
MAY, 1985

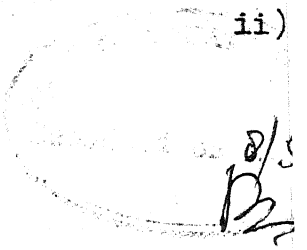

CERTIFICATE

Certified that the present work entitled, 'Characterisation and Beneficiation of Kudremukh Iron Ore Tailing' by S.A.Ravishankar has been carried out under my supervision and has not been submitted elsewhere for a degree.

May, 1985.

A. K. Biswas

(A.K.Biswas)
Professor
Department of Metallurgical Enginee
Indian Institute of Technology, Ka

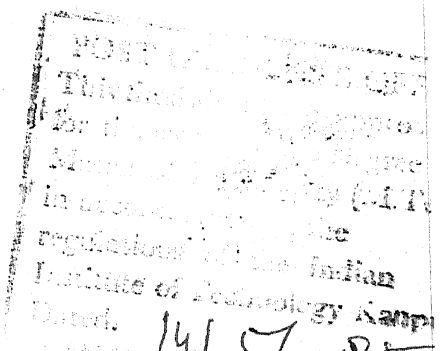

ACKNOWLEDGEMENTS

I express my deep sense of indebtness and gratitude to Dr.A.K.Biswas who proposed, guided and helped this work to thrive through his uncountable suggestions and constructive criticisms.

I am thankful to Dr.K.S.Gandhi, Dr.R.K.Ray and Dr.N.K.Khosla for their immense help in my experimental difficulties.

I am thankful to Kudremukh Iron Ore Corporation Ltd. for providing the material.

I am grateful to Mr.S.C.D.Arora, Mr.Mongole, Mr.Jain, Mr.Das and Mr.Uma Shankar for their technical help.

I am grateful to my friends Mr.Rakesh Kumar and Miss Uma Devi without whose timely assistance the work would not have been completed in time.

I am also thankful to my friends Mr.Raman, Mr.V.Swamy, Mr.Ramamoorthi and Mr.Venkatesh for the lively company.

Last but not the least I am thankful to Mr.U.S.Misra for his fast and fastidious typing.

-S.A.RAVISANKAR

CONTENTS

LIST OF TABLES

LIST OF FIGURES

ABSTRACT

This work was motivated to thrive a route to beneficiate the 46% of the total raw material, which is getting dumped as spiral tail (of grade 33% Fe) after the beneficiation of magnetite rich Kudremukh Iron Ore. The work started with the liberation studies followed by characterisation studies and finally the beneficiation studies. It was found in the liberation studies that the liberation was almost consumate below 147μ . Characterisation studies were carried out by XRD and TEM. Micro hardness studies coupled with XRD was carried out to characterise the ore. Apart from the major phases magnetite, hematite, goethite, Maghemite and quartz many new minor phases have been identified such as alunite, calcium aluminum silicate, wustite, collinsite, lepidocrocite, akaganite etc.

Beneficiation studies were initiated with pure minerals and pursued extensively with actual spiral tail of Kudremukh Ore. The studies were started with magnetic separation which gave ~ 5% of concentrate assaying 98.1%. The nonmagnetic fraction was brought to 0-74μ size range and then subjected to selective flocculation and settling experiments. The flocculants used were starch, amylopectin, polyacrylamide of different molecular weight and xanthate introduced polyacrylamide. The other variables studies were pH, and dispersant concentration. The best grade (59% Fe_2O_3)

obtained in 0-74μ particle system was with zanthate introduced polymer. The recovery in this case was 48%. When the particle system was reduced to 0-20μ, the best grade (78% Fe_2O_3) with recovery 76.50% was obtained with zanthate introduced polymer.

Settling studies results were performed at different pH and dispersant concentration. The best grade obtained was 65% Fe_2O_3 and recovery (70.98%). In the cases of selectivity index $S_I = \sqrt{\frac{R_{vm}}{(100-R_{vm})} \times \frac{R_{lvm}}{(100-R_{lvm})}}$ appropriately defined in the text was calculated and taken as a measure of separability.

CHAPTER 1

PREAMBLE

Kudremukh is one of the richest sources of magnetite ore. It is in Karnataka state 63 km away from Mangalore port. The iron ore deposits in Kudremukh, part of Kudremukh - Aroli Gangamila range, were discovered in 1913 by late P.Iyengar a renowned Geologist in Mysore state, but came to light only in 1966.

The ore is mainly a magnetite material with hematite, martite as their other major iron bearing mineral. Silica the important gangue mineral may present upto 18 pct as silicate minerals. The ore has several minor phases like goethite, limonite, vivianite, psilo melane, grunenite etc. The ore consists of two part, one soft weathered ore at the crust and another inner core of ore body. In between there is a zone of transition which represents intermediate state of weathering.

The iron ore beneficiation plant is situated in Kudremukh, a small town ship. The plant treats 23712 tph of -7" ROM containing 39% + Fe. As shown in the plant flow sheet (Fig.1), after communition and grinding of ROM, it is treated in magnetic separators followed by rougher and cleaner spiral. Finally it goes to thickners where the water is removed for reuse. Concentrates are removed from

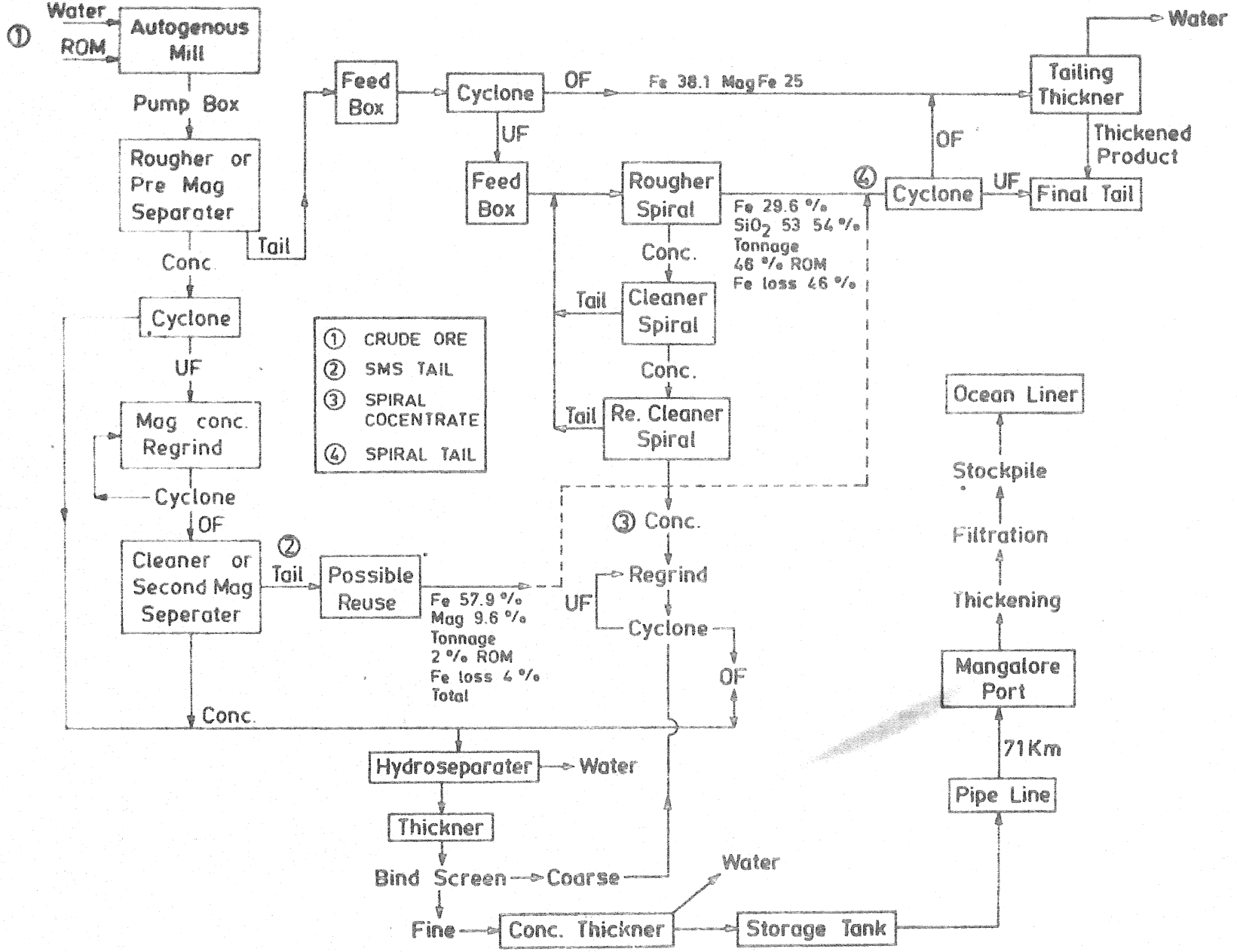
Water
ROM
Autogenous Mill
Pump Box
Rougher or Pre Mag Separater
Tail
Conc.
Cyclone
UF
Mag conc. Regrind
Cyclone
OF
Cleaner or Second Mag Seperater
Tail
Possible Reuse
Conc.
Feed Box
Cyclone
OF
Fe 38.1 Mag Fe 25
UF
Feed Box
Rougher Spiral
Conc.
Tail
Cleaner Spiral
Conc.
Tail
Re. Cleaner Spiral
Fe 29.6 %
SiO2 53 54 %
Tonnage
46 % ROM
Fe loss 46 %
Cyclone
OF
UF
Final Tail
Water
Tailing Thickner
Thickened Product
① CRUDE ORE
② SMS TAIL
③ SPIRAL COCENTRATE
④ SPIRAL TAIL
Fe 57.9 %
Mag 9.6 %
Tonnage
2 % ROM
Fe loss 4 %
Total
③ Conc.
Regrind
UF
Cyclone
OF
Hydroseparater
Water
Thickner
Bind Screen
Coarse
Fine
Conc. Thickner
Water
Storage Tank
Ocean Liner
Stockpile
Filtration
Thickening
Mangalore Port
71 Km
Pipe Line

primary magnetic and secondary magnetic separators. Approximately 7.5 mtpy of concentrate with 65-66% Fe, 4.0-4.5% SiO_2, < 1% Al_2O_3, 0.02-0.04% S and 0.03-0.05 P is being removed through the present set of beneficiation equipments.

The material of interest, in this thesis is spiral tail obtained after roughing action by spirals. About 46% of the ROM is getting removed as spiral tail containing 29.8% Fe. Totally 11664 tph are getting dumped as spiral tail (4) in Fig.1 .

Though there are two kinds of tail one spiral tail (Ref. Fig.1) and another secondary magnetic separator (SMS) tail. But in this thesis importance was given to spiral because of the following reasons:

(1) Fe loss is much more compared to SMS tail. The total Fe loss in spiral tail and SMS tail are in the ratio of 12 : 1.

(2) Weight loss is 46% of ROM in case of spiral tail and only 2% of ROM in SMS tail.

The tailings contributing almost 46% of the total ROM, that too with Fe content 29.8%is very undesirable and it really posses a challenge to the efficiency of the plant.

The main objective of this work is to beneficiate this spiral tail, to blast furnace grade, preceded by liberation

and characterisation.

Liberation studies were carried out using a high resolution optical microscope to obtain an idea about the physical association of minerals in the material of interest. Phase characterisation studies were done to find out the minerals present both valuable and gangue. The techniques adopted in this study are X-ray and transmission electron microscopy. Liberation and phase characterisation studies also helped in selecting the beneficiation techniques. Beneficiation techniques used were mainly magnetic separation, selective flocculation settling and flotation. The selective flocculation studies were done with variablespH, flocculant concentration and flocculant itself.

CHAPTER 2

PETROLOGICAL STUDIES ON KUDREMUKH IRON ORE TAILING

Petrological studies were carried out on different size fractions of the samples of spiral tail to find out the extent of liberation for further beneficiation and other important details about hardness, grain size and the size of the locked minerals.

(a) To find out the liberation datas and the nature of locked minerals the particles of different size fraction were sprinkled on the glass slide and observed through optical microscope. Each time some 30-40 particles were observed in the frame. The results are tabulated in Table 2A.

(b) To find out the grain size, hardness and typical size of the locked particles the representative sample particles picked up by hand were mounted by use of a cold setting resin. The mounted resin was then polished in an automatic polishing machine. The polished sample was examined under optical microscope. The sample was then etched with HF to reveal other details.

TABLE 2A

LIBERATION STUDIES

Size Range	Locked/Liberated	Remarks
-35 + 48	Locked/70% of the total particles seen	(1) At this stage there were some black particles fully liberated (2) Some small inclusions of quartz were also seen, showing incomplete liberation.
-48 + 65	Locked/20% of the total particles seen	The liberation was fairly good. There were some locked white particles in the red and black matrix. But liberated black and white particles were seen in significant amount.
-65 + 100	Locked materials are in relatively very small amount (10%)	Liberation had improved significantly. Well liberated particles are seen through out
-100 + 200	Liberated	The liberation is sumptuous for practical purposes. But still few particles in the frame were seen unliberated.

2.1 Some of the Salient Features Seen

(1) The locking black and white particles in red matrix and vice-versa was seen (Ref. Figs. 2.1 to 2.5).

(2) The typical grain size of each black and white particles locked in the red matrix which were supposed to be the smallest grain locked in the matrix.

(3) Some red phase were found along the grain boundary of quartz (Fig.2.6).

(4) Grain size information of brown and red particles were found out (Figs. 2.7, 2.8).

Grain size of Brown particle - 25μ

Red particle - 10 μ

(5) Micro structure of black material had been photographed (Ref. Figs.2.9, 2.10).

2.2 Micro Hardness Measurements

The hardness of a mineral is measured by the resistance which a smooth surface offers to abrasion. Accurate determinations of the hardness of minerals can be made in various ways, one of the best being by use of an instrument called scherometer. But in this work an abacus for finding micro hardness with the optical microscope was used. Though there was a large scattering of hardness values of the same particle, their range and maxima,minima were well distinguishable from the other particles/phases.

The relation of hardness to chemical composition was exploited to find out the probable phases present in the different particles. Table 2B and 2C shows the micro hardness of different coloured materials and the probable phases.

Micro hardness was calculated in Vicar's scale using the formula

$$\frac{1854.4 \times P}{D^2}$$

D- microns

P- weight

TABLE 2B

MICRO HARDNESS STUDIES

Color of the particle	Micro hardness kg/mm^2	Probable phases	Remarks
White	205.47 - 136.22	Alumino-silicates and silicates	From the X-ray these particles have proved to be pure quartz
Black	32 - 64	Magnetite and maghemite, and goethite (generally oxides of iron)	From the X-ray, it has been revealed that black particles are magnetite and maghemite concentrates
Red	49 - 110	Mostly gangue minerals with iron bearing minerals like Hematite, Maghemite	This is proved by X-ray methods.

TABLE 2C

MICRO HARDNESS STUDIES

Colour of the particle	Details	Hardness kg/mm^2	Probable phase and Remarks
Dull Red/ particle	Indentation was made on a white particle in the red matrix	144 - 189	Shows the presence of quartz
	Indentation was made on black particle	45 - 52	From the colour it was a magnetite rich phase. But the decreased hardness was accounted by the fact that the supporting matrix was softer than the black particle
Black particle	Very porous - and indentation was made on a plane surface	87 - 121	Suspected to be an intimate mixture of quartz magnetite, goethite and maghemite. X-ray also revealed the same
Brown particle	On different spots of the particle	32 - 35	Could be some hematite, goethite etc.

Continued....

TABLE 2C (Continued):

Colour of the particle	Details	Hardness kg/mm^2	Probable phase and Remarks
	On black particles found along the grain boundary of the brown phase	32 - 36	Could be magnetite particles
	On a red phase found at a region in the brown particle	13.- 37	Shows the presence of hematite X-ray diffraction of brown particle also proved the above facts. These particles are found to contain magnetite, hematitte, maghemite etc. with traces of gangue mineral.

CHAPTER 3

X-RAY DIFFRACTION STUDY

X-ray diffraction studies were carried out on samples supplied by Kudremukh iron ore corporation. The samples (a) crude ore, (b) SMS tail, (c) spiral concentrate, (d) spiral tail are analysed by Iso-Debye-Flex 2002 diffractometer. A small amount of powder sample (-200 mesh) was taken in a perspex specimen holder and mounted on the specimen stage of the diffractometer. CuK^{α} radiation with Ni filter was used and the intensity vs 2θ plots were recorded on a chart paper.

3.1 Preamble to X-ray Diffraction Work

The x-ray diffraction pattern from the received sample was shown in Fig.3.1. The interplaner spacings 'd' were calculated from Bragg's law $\lambda = 2d\sin\theta$ where λ = wavelength of the characteristics radiation used ($\lambda = 1.542$ A°) and θ is the angle at which Bragg reflection takes place which was obtained from the diffraction peaks. The relative intensities were also calculated. Attempts were made to identify the minerals by comparing the first three strongest 'd' values with those of the various possible mineral. But due to the presence of large number of phases, it was not possible to do so. So corresponding to each 'd' value, a

list of probable compounds whose one of the 'd' values lies within ± 0.015 A° was made as shown in Table 3 (A,C,E,G). Hence such a list against each 'd' value with take into account all probable phases that might present in the sample. Finally the number of times a phase had appeared was also listed in Table 3 (B,D,F,H). The higher the number of appearances, more was the possibility of existing that phase. However the presence of such phases were independently verified by electron diffraction. The spiral tail sample was subjected to magnetic separation and x-ray diffraction patterns were shown in Fig.3.2. The different coloured particle were separated by hand picking and their patterns were given in the Fig.3.3. The sample was digested in hydrochloric acid, to remove major iron bearing minerals and the x-ray diffraction pattern for gangue minerals were found out.

3.2 X-ray Diffraction Patterns of the Samples as Received

The samples crude ore, (a) spiral concentrate (b), secondary magnetic separator tail (c) and spiral tail (d) were analysed by x-ray and the patterns were given in Fig.3.1. In all the above four materials the peak at 26.6° was found which corresponds to quartz. The intensity was maximum in case of spiral tail. Besides a, b and c in Fig.3.1 have a strong peak at 2.69Å which was

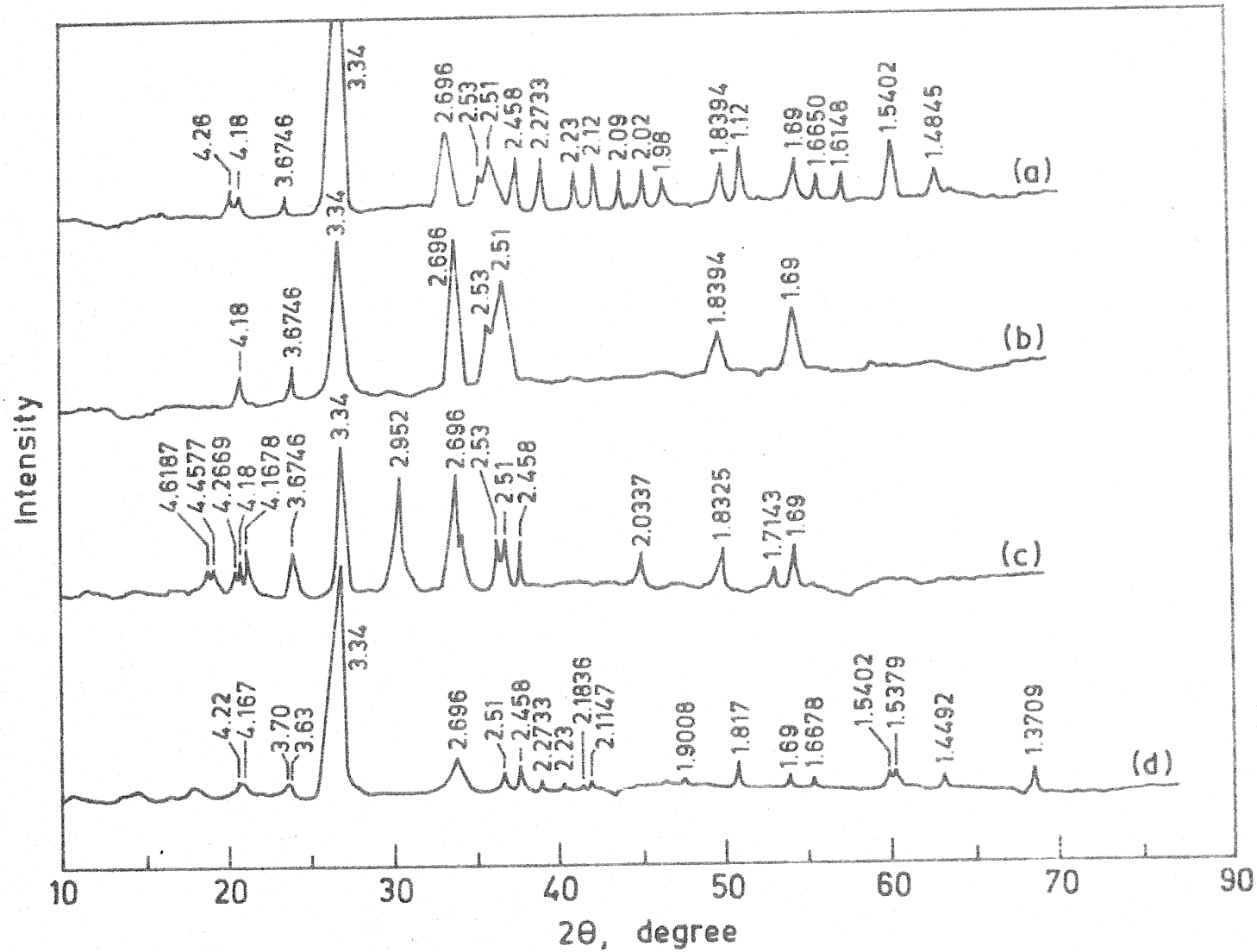

Fig. 3.1. X-ray diffraction patterns of crude ore (a), spiral concentrate (b), secondary magnetic seperator tail (c), and spiral tail (d) as received material.

very weak in spiral tail (d). The intensity of peak at 26.6° increases in this order spiral tail crude ore SMS tail spiral concentrate. Similarly the intensity of the peak at 33.3° is 20 in case of (a) crude ore and 12 in case of spiral tail. The intensities of other peaks are low and have not changed appreciably.

3.3 X-ray Diffractions from Spiral Tail

The spiral tail material was powdered in a ball-mill in a controlled rate and subjected to magnetic separation. The x-ray diffraction patterns of non-magnetic (a) and magnetic (b) fractions are given in Fig.3.2. The intensity of peak at 33.3° has increased from 25 to 80 when compared nonmagnetic fraction with magnetic fraction. The peak at 26.6° has decreased from 100 to 50 when compared nonmagnetic fraction with magnetic fraction. There is a new peak in case of magnetic fraction at 30.5°. Many peaks found in non-magnetic fractions were absent in magnetic fraction.

The results are tabulated in Tables 3 (I, J, K, L).

3.4 X-ray Diffraction Patterns from Spiral Tail

This three patterns in Fig.3.3 are to give some idea about the liberation and also what phases are concentrated in a particular coloured particle. This patterns (a) was obtained by picking some typical black coloured particles

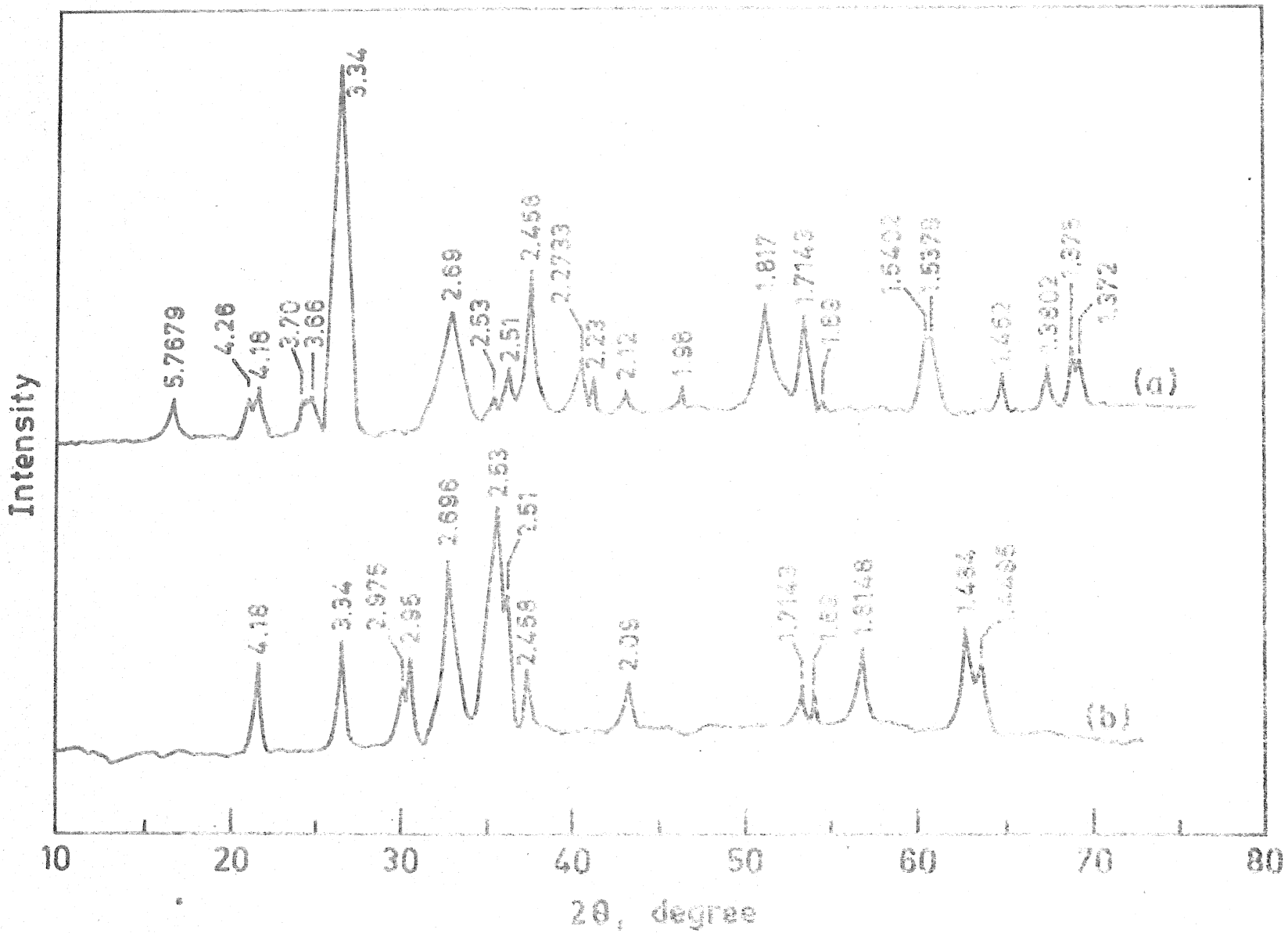

Fig. 3.2. X-ray diffraction patterns of (a) non magnetic fraction (b) magnetic fraction of spiral tail.

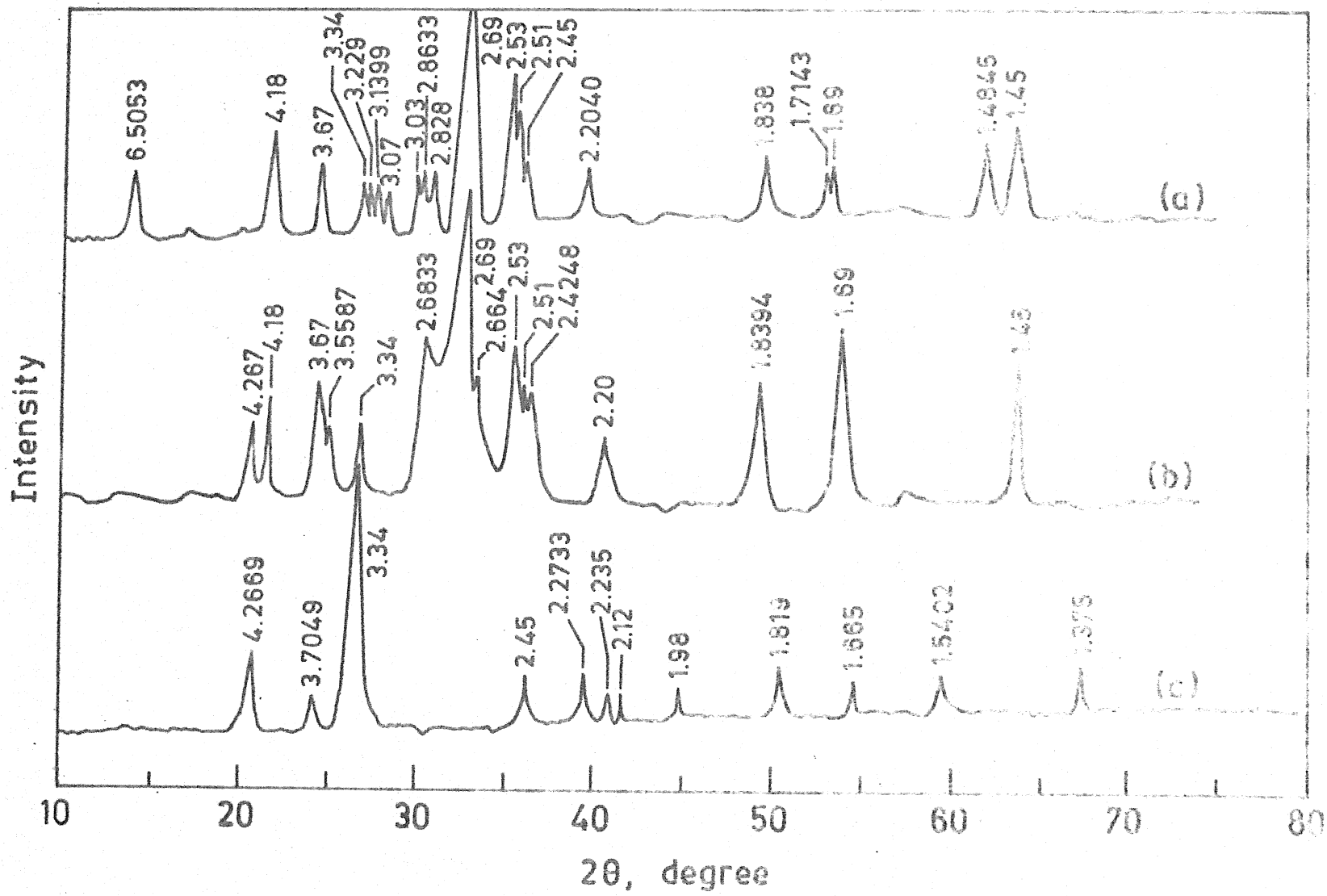

Fig. 3.3. X-ray diffraction patterns of Black Material (a) red particle (b) colourless white material (c) from spiral tail.

similarly (b) with red coloured and (c) with white coloured. In red and black coloured particles the peak at 33.3° is much more pronounced when compared to white particle. The peak at 35.4°in black particle is more pronounced compared to red particle showing that black particles are essentially magnetite concentrates. The peaks which are found in red and black particles at 40.8°, 54.3° and 64.5° are not found in whiite particle. Similarly some peaks which are found in white particles at 39.6°, 40.4°, 42.5°, 50.3°, 55.1° and 60° which characteristic low intensity peaks for quartz are not found in black and red particles. The results are tabulated in 3 (M, N, O, P, Q).

CHAPTER 4

TRANSMISSION ELECTRON MICROSCOPY STUDIES

Transmission electron microscopy work was carried out on samples of Kudremukh; (a) crude ore, (b) SMS tail, (c) spiral tail, (d) spiral concentrate using Philips EM-301 electron microscope operated at 100 kV. The microscope can be operated at different accelerating voltage i.e. 20 KV, 40 KV, 60 KV, 80 KV and 100 KV. The maximum attainable magnification is X 2,000,00 but the recording in film takes place at maximum X 63,000. The specimen stage of the microscope can be fitted with respect to electron beam to an angle 0° to 45°.

A few grams of representative powdered samples were suspended in acetone and subjected to ultrasonic viberations in an ultrasonic cleaner for 15 minutes. After allowing the suspension to settle, a drop of the supernatant liquid was put on a thin (~ 500 A°) carbon film supported by a 3 mm dia 200 mesh. copper grid. Since the material being para-magnetic in nature, the specimen must be sandwiched between 2 carbon films. The sample loaded copper grid was coated once again with a carbon coating apparatus. Now the latter was mounted on the specimen stage of the electron microscope for identification of the minerals present in the samples by selected area electron diffraction. Thin areas of the

particles were examined in the selected area diffraction mode and the specimen was titled if necessary with respect to the electron beam between 10° and 40° in order to get sharp diffraction pattern.

For analysis of the diffraction patterns, three vectors R_1, R_2 and R_3 (distances from the centre of the pattern to the nearest diffraction spots) were measured and then the interplanar spacings (d) were calculated from the relation $Rd = L\lambda$ where R was the magnitude of the vector, d, the interplaner spacing and $L\lambda$, the camera constant. The value of $L\lambda$ was obtained by measuring the radius R of the diffraction rings obtained from gold sample under the same conditions on which the diffraction patterns from the sample were taken. Since gold has structure the relation $Rd = L\lambda$ can be written as

$$R \cdot \frac{a}{\sqrt{h^2 + k^2 + l^2}} = L\lambda$$

where a = lattice parameter of gold

or

$$R = \frac{L\lambda}{a} \sqrt{h^2 + k^2 + l^2}.$$

Hence R vs. $\sqrt{h^2 + k^2 + l^2}$ plot gives a straight line passing through origin the slope of which gives $L\lambda/a$. Since 'a' is known $L\lambda$ was determined.

Now the three 'd' values, so obtained, were matched with those of all various possible minerals. The angle between the planes were also calculated and if it matched with the angle measured on the diffraction pattern, then it can be said that diffraction pattern corresponds to that mineral.

ANALYSIS OF DIFFRACTION PATTERNS

4.1 Diffraction Pattern from Sample of Kudremukh

Figure 4.1 showed the diffraction pattern from one particle of the sample. The three vectors R_1, R_2 and R_3 was found to be 0.87, 0.87, 1.5 cm. respectively. The interplanar spacing were calculated from the relation $Rd = L\lambda$ where $L\lambda$. Camera constant which was calculated from a standard sample quartz examined under the same conditions on which the diffraction patterns was taken.

The gold pattern was analysed and used as a standard pattern to standardise quartz.

R(cm)	R^2	R^2/R^2 Min	$h^2+k^2+l^2$	$\sqrt{h^2+k^2+l^2}$	$R\sqrt{h^2+k^2+l^2}$
0	0	0	0	0	0
2.8	7.84	1	3	1.732	4.8496
3.2	10.24	1.306	4	2	6.400
4.56	20.7936	2.652	8	2.828	12.8956
5.35	28.6225	3.650	11	3.317	17.74595
=15.91			= 26	= 9.877	= 41.891

From regression line analysis

$$\text{Slope} = \frac{L\lambda}{a} = \frac{1}{2}\left(\frac{n\Sigma R\sqrt{h^2+k^2+l^2} - \Sigma R\,\Sigma\sqrt{h^2+k^2+l^2}}{n\Sigma(h^2+k^2+l^2) - (\Sigma\sqrt{h^2+k^2+l^2})^2}\right)$$

$$= \frac{1}{2}\left(\frac{5\,(41.89115) - (157.143}{5(26) - 97.555}\right) = 0.806175$$

$L\lambda = 0.806175 \times 4.0783 \quad a = 4.0783\ A^\circ$

$= 3.287827\ \text{cm}\ A^\circ$

The error was calculated in Appendix A.

From the camera constant the interplanar spacing d_1, d_2 and d_3 were found to be 4.26 A°, 4.26 A° and 2.458 A°.

The angle between the vectors

$$R_1 \quad R_2 = 60^\circ$$

$$R_1 \quad R_3 = 30^\circ$$

These interplanar spacings were found to match well with the SiO_2 quartz within 1.5 pct. accuracy.

	Measured	SiO_2	hkl	(hkl) selected
d_1	4.26 A°	4.26 A°	(100)	(100)
d_2	4.26 A°	4.26 A°	(100)	(010)
d_3	2.458A°	2.458A°	(110)	(110)

The beam direction [001].

Crystal structure of SiO_2 is hexagonal.

The angle between the plane (100), (010)

$$\text{Cos } \phi = \frac{h_1h_2+k_1k_2 + \frac{1}{2}(h_1k_2+h_2k_1) + \frac{3a^2}{4c^2} l_1l_2}{\sqrt{(h_1^2 + k_1^2+h_1k_1 + \frac{3a^2}{4c^2} l_1^2)(h_2^2+k_2^2+h_2k_2+ \frac{3a^2}{4c^2} l_2^2)}}$$

$$a_o = 4.913, \quad c_o = 5.405.$$

Substituting these values the angle was found to be 60° against 60° as measured from diffraction pattern.

Similarly angle between(100) and (110) was found to 30° against 30° as measured from diffraction pattern.

Since the interplanar spacing and angle between the vectors were found to fit very closely to these of SiO_2, it was concluded that the pattern was from SiO_2 (quartz).

Figure 4.2 showed the corresponding micrograph of the particle from which the diffraction pattern was obtained. The size of the particle is

Figure 4.3, the three vectors R_1, R_2 and R_3 were measured to be 0.65 cm, 1.825 cm and 2.00 cm respectively and the interplanar spacing were found to be 5.67 A°, 2.019A° and 1.842 A°.

The angles between the vectors:

$$R_1 \quad R_2 = 86°.30'$$

$$R_2 \quad R_3 = 19°.$$

These interplanar spacings were found to fit with alunite (K, Na) $Al_3(OH)_6(SO_4)_2$ (system-hexagonal, $a_o = 6.97$; $c_o = 17.38$) and they were 5.76A° from plane $(01\bar{1})$ 2.04 A° from plane (018) and 1.90 from plane 027 . The angles between $(01\bar{1})$ and (018), $(01\bar{1})$ and (027) were calculated to be 88°6' and 19°36' respectively. Beam direction is [100].

The corresponding micrograph of the particle is shown in Fig.4.4 cited its size is

In Fig.4.5, the vectors R_1, R_2 and R_3 were measured to be 0.51666 cm, 1.475 cm and 1.575 cm respectively and the interplanar spacings d_1, d_2 and d_3 were calculated to be 7.1332 A°, 2.4986 A° and 2.340 A° respectively. The angles between the vectors were as follows:

$$R_1 \quad R_2 = 93°$$
$$R_1 \quad R_3 = 73°$$

The d values were found to match with those of maghemite $-Fe_2O_3$ (system tetragonal $a_o = 8.33$, $c_o = 24.99$) and they were 7.04 A° (from plane $(\bar{1}11)$, 2.45 A° (from plane (314)) and 2.31 A° (from plane 306) respectively. The beam direction is $[\bar{2}21]$. The angles between the planes $(\bar{1}12)$ and (306), (314) and (306) were calculated to be 72°10' and 19°26'.

The corresponding micrograph of the particle is shown in Fig.4.6 and the size is

In Fig.4.7 the vectors R_1, R_2 and R_3 were found to be 0.895 cm, 0.0866 cm and 1.4 cm respectively. The corresponding 'd' values calculated were 2.295 A°, 1.8902 A° and 1.4672 A°. These values were found to match very closely to those of pyrite FeS_2 (system cubic $a_o = 5.417$ A°) and they were 2.2119 A° (from plane $(1\bar{1}2)$), 1.9155 A°

from plane 220 and 1.4478 A° from plane 312 respectively. The angles between the planes $(1\bar{1}2)$ and (220), $(1\bar{1}2)$ (312) were found to be 90° and 49°6' respectively against measured 90° and 50° from the diffraction pattern. The beam direction is $[\bar{1}11]$.

The micrograph is given in Fig.4.8 and the grain size is

In Fig.4.9, the vectors R_1, R_2 and R_3 were found to be 0.66 cm, 1.15 cm, and 1.385 cm respectively. The corresponding 'd' values calculated were 1.7334A°, 3.08A° and 1.4831A°. These values were found to be match very closely to those of magnetite Fe_3O_4 (system-cubic, a_o = 8.3967) and they were 2.967A° (from plane $0.2\bar{2}$), 2.967A° (from plane $02\bar{2}$) and 1.4845A° (from plane 440). The angles between $(02\bar{2})$ and (422), (422) and (440) were 90° and 30° respectively against measured 86°30' and 28°. The beam direction is $[1\bar{1}\bar{1}]$.

The micrograph is given in Fig. 4.10 and the grain size is

In Fig.4.11, the vectors R_1, R_2 and R_3 were found to be 0.8 cm, 1.48 cm and 1.9 cm respectively. The corresponding 'd' values calculated were 2.6245A°, 1.4186A° and 1.105A°. These values were found to match very closely with goethite $Fe_2O_3H_2O$ (system orthorhombic, a_o = 4.596, b_o = 9.957 and c_o = 3.021 and they were 2.69A° (from plane 130) 1.418 (from

plane 112) and 1.12A°(from plane 242) respectively. The angles between the planes (130) and (112), (130) and (242) were 72°44' and 49°12' respectively against measured 70° and 46° from the diffraction pattern. The beam direction is [$\bar{3}$11].

The micrograph is given in Fig.4.12 and the grain size is

In Fig.4.13 the vectors R_1, R_2 and R_3 were found to be 0.636 cm, 1.05 cm and 1.13 cm respectively. The corresponding 'd' values calculated were 3.3012A°, 1.999A° and 1.858A°. These values were found to match very closely to those of Akaganite FeOOH (system Tetragonal, a_o = 10.48, c_o = 3.023) and they were 3.311A° (from plane 3$\bar{1}$0), 2.064A° (from plane 150) and 1.854A°(from plane 440) respectively. The angles between the planes (3$\bar{1}$0) and (150), (3$\bar{1}$0) and (440) were 97°7' and 63°26' against measured 95°30 and 62° from the diffraction pattern. Beam direction is [001].

The micrograph is in Fig.4.14 and the grain size is

In Fig.4.15, the vectors R_1, R_2 and R_3 were found to be 0.69 cm, 0.6833 cm and 1.00 cm respectively. The corresponding 'd' values calculated were 2.87A°, 2.89A° and 1.9809A°. These values were found to match very closely to those of Calcium Aluminum Silicate $CaAl_2SiO_6$ (system - Monoclinic, a_o = 9.619, b_o = 8.659, c_o = 5.278, = 106°14') and they were

2,94A' (from the plane $\bar{2}21$ and $\bar{2}\bar{2}1$) and 2.005A°(from plane $\bar{4}02$) respectively. The angles between the planes ($\bar{2}21$) and ($\bar{2}\bar{2}1$), ($\bar{2}21$) and ($\bar{4}02$) were found to be 85°44' and 43°5' against 86° and 44A° measured from the diffraction pattern. The beam direction is [102] .

The micrograph of the pattern is given in Fig.4.16 and the grain size is

In Fig.4.17, the vectors R_1, R_2 and R_3 were found to be 0.5333 cm, 0.685 cm and 1.015 cm respectively. The corresponding 'd' values calculated were 3.7141A°, 2.8919A° and 1.9516A°. The values were found to match very closely to those of $FeSiO_3$ (system - orthorhombic, a_o = 18.3, b_o = 9.13, c_o = 5.2) and they were 2.596A° from plane ($13\bar{1}$) , 2.134 (from plane (502) , 1.350 from plane (633) . The angles between (131) and (502), (502) and (633) were found to be 60°40' and 26°57' against measured 65 and 30° from the diffraction pattern. The beam direction is [$21\bar{5}$].

The micrographs in Fig.4.18. The grain size is

In Fig.4.19, the vectors R_1, R_2 and R_3 were found to be 1.925 cm, 1.40 cm and 2.45 cm respectively. The corresponding 'd' values calculated were 1.6860A°, 2.348A° and 1.3419A°. The values were found to match very closely to those of Wustite FeO (system-cubic, a_o = 4.307) and they were 1.523A° (from plane 220), 2.153A° (from plane 002) and 1.241A° (from plane 222). The angles between (220) and (002),

(002) and (222) were found to be 90° and 54°45' against measured 87° and 52°. The beam direction is [110].

The corresponding micrograph is shown in Fig.4.20. The size of the grain is

In Fig.4.21, the vectors R_1, R_2 and R_3 were found to be 0.7675 cm, 0.81666 cm and 1.25 cm. The corresponding 'd' values calculated were 2.579A°, 2.4255A° and 1.58472A°. The values were found to match with those of $-Fe_2O_3$ Maghemite (system-cubic, a_o = 8.350) and they were 2.52A° (from the plane $3\bar{1}\bar{1}$), 2.41A° (from the plane 222) and 1.61 (from the plane 511) respectively. The angles between the planes $(3\bar{1}\bar{1})$ and (222), $(3\bar{1}\bar{1})$ and (511) were 79°58' and 41°1' respectively against measured 78° and 40° from the diffraction pattern.

The beam direction is $[01\bar{1}]$.

The micrograph is given in Fig.4.22. The grain size is

CHAPTER 5

BENEFICIATION STUDIES

5.1 Introduction

The problem in Indian Iron Ore is two fold, one being the high alumina content and the other being the soft nature of the minerals which generates considerable amount of fines during mixing and handling. Besides these problems, fines are produced during the conventional communition, grinding and beneficiation processes. Indian Iron Ores are relatively soft in nature and the introduction of mechanisation and heavy blasting of mines is generating larger quantity of fines[1,2,3,4]. The proportion of -10 mm fines from Indian mines are never less than 35% and likely to increase when mixing is carried out at greater depths. These fines are of inferior quality for smelting as such in the blast furnace. Moreover they can not be treated in the blast furnace since it requires close sizing of lumps ore.

The Kudremukh iron ore is very rich in magnetite. The ferromagnetic character of this mineral is exploited in magnetic separation. The technical literature includes[5] the details of both wet and dry low intensity separators and their applications. The wet separators are the most common. They employ either electromagnets or permanent magnets. Further, general literature on wet high intensity magnetic

separators are available[6,7,8]. Dry magnetic separators also employ eitherelectromagnets or permanent magnets. Detailed literatures[5] are available about the recent advancements.

When the liberation is good enough and particles size is not very fine then one can adopt the magnetic separation, gravity separation and even flotation if the size range is -100 mesh. The major problem with particle size when it is ultra fine is its poor response to the (above said) physical separation techniques.

Of late, of the processes one that appears quite promising for the fine particle separation, is "selective flocculation". Ideally this should involve the agglomeration of desired mineral species into flocs leaving the other particulate species in suspension. Separation of flocculated material by processes such as flotation, sedimentation or elutriation should result in the desired concentration[10,11]. The success of the technique of separation by selective flocculation depends on the separation particulates from each other, preferential adsorption of flocculants on particles and bridging of these into flocs by the adsorbed polymer molecules, and effective separation of the flocculated mass from the suspension using a technique that will not produce redispersion of flocs.

Fine particles constituting a mineral mixture usually have a tendency to coat each other and, thus, the selectivity in flocculating a particular mineral is significantly lowered[9]. This problem of slime coating and heterocoagulation is usually overcome by the use of dispersants which prevent interparticle adhesion. Atleast one component should be well dispersed[9]. The second requirement, the essence of the process, is that a flocculant selectively gets adsorbed on only one of the constituents of the mixture. Selective flocculation then follows, after which the flocs of one component can be removed from a dispersion of the other mineral.

The force responsible for adsorption of polymers is mainly due to three types of bonding namely, electrostatic, hydrogen and covalent bonding[11]. The predominance of any of the above mechanisms over the other depends on the particular mineral polymer system and the properties of the aqueous medium. Under favourable conditions, more than one type of mechanism could be operative.

Reported work on selective flocculation has been performed with binary minerals[9]. Hematite quartz system has been studied by many workers using starch or polyacrylamides as flocculant and sodium silicate as dispersant[9,10,11]. Beneficiation of multicomponent natural ores by selective flocculation has been attempted by Frommer et al[13],

Dicks et al[14], Iwasatu et al[15] and Guraraj et al[16]. In a few component natural ores by selective flocculation[11], commercial development of Tilden's billion ton iron ore deposit is a major break through in concentration technology and is the first commercial application of this technique[17,18]. Starch and sodium silicate have been used as flocculant and dispersant respectively for the beneficiation of Tilden mine ore which is ground to 85% minus 500 mesh (25μ)[19]. Tilden ore body has grain size less than 25μ and so the liberation of minerals would occur only at very low particle sizes.

Besides, much works are being carried out in Lake Superior District having a large potential reserve of iron to develop methods for treating oxidised taconites by selective flocculation-desliming followed by cationic or anionic flotation of gangue minerals[20].

At the Twin cities Metallurgy Research Center, selective flocculation of the iron minerals followed by the cationic flotation of the gangue minerals are being used to develop the iron potential of the Western Mesabi range oxidised taconites[14].

The effects of hard water and the influence of calcium, magnesium ions on flocculability were extensively studies by Krishnan and Iwasaki[21].

5.2 The Objective of the Work

The objective of this work in the beneficiation studies is to thrive the beneficiation through 4 techniques namely magnetic separation, selective flocculations, settling and flotation studies. The primary reason for selecting the above methods is the encouraging results from liberation studies which apprised good a degree of liberation below 100 mesh. The secondary reason for selecting settling, flocculation and flotation is the clear discrimination in their density values and crystal structure. Though flotation result didn't give any good result, it is possible to try with different collector which will be exclusively selective for quartz.

5.3 Materials and Methods for Beneficiation Studies

The details of chemicals and the materials used are mentioned below:

(i) Materials: (a) Pure Hematite, pure Magnetite, pure quartz

(b) Spiral tail* and crude ore** of Kudremukh Iron ore Corporation Ltd.

The size analysis and chemical compositions of spiral tail are given below:

---

*,** These materials are shown in the flowsheet (Fig.1).

Size Analysis of Spiral Tail

Size range (mesh)	wt %
-6 + 20	8.0
-20 + 35	10.5
-35 + 65	15.3
-65 + 100	12.5
-100 + 200	37.6
-200 + 325	10.9
-325	5.2

Chemical Composition of Spiral Tail

Total Fe%	29.8%
Magnetite	1.79%
Hematite	17.98%
Goethite & Limonite	25.79%
Silica	53.14%

besides it contains some alumina, MnO etc.

(ii) Chemicals:

Flocculants:
(i) Starch
(ii) Polyacrylamide of different molecular wt
(iii) Amylopectin
(iv) Zanthate introduced polyacrylamide.

Dispersant: Sodium silicate

pH controller: NaOH & HNO_3.

The Magnetite material was procured from LKV Sweden.

5.3.1 Size Fractionation of Spiral Tail Particles

In order to study the size distribution of spiral tail, the received material was subjected to wet sieving using the laboratory shaker. Then each size fractions is weighed and assayed for further studies. The Table 5B shows the typical size distribution of the spiral tail received as such.

5.3.2 Grinding of the Spiral Tail

For coarse grinding the laboratory ball mill was used by loading the ball mill with iron balls. The size and number of balls were chosen in such a way that they produce less fines and bring all the materials below 110μ.

Fine grinding was done by feeding the material ground, as mentioned in the previous method in a planetary ball mill (Fitsch GmbH West Germany) using stainless steel balls. It was allowed to run for 4 hrs to bring the material below. The particle size distribution of this grounded material was found out using coulter counter. Table 5A shows the particle size distribution of the material ground in the planetary ball mill.

5.3.3 Methods of Preparation of Flocculants

Different Methods Preparation of Starch Solution Used in this Work

From the literature survey it was found that there are different methods for preparation of starch solution. Out of those methods some of the important methods were used for the preparation of starch solution.

5.3.3.1 Modified Causticized Homogenised Method (MCH)

0.5 gm of commercial starch was taken in a 500cc beaker and then 3cc of distilled water was added to it. The agglomerates were broken down by a glass rod. Then 3cc of 0.5 (N) NaOH was added and 0.5 (N) NaOH was again added and a thick gel was formed by stirring with glass rod for 1 minute and then stirring was stopped and gel was kept for 6 minutes. After this 1cc of water was added and the gel was mixed with glass rod. Water was slowly added and the gel was mixed with glass rod and the volume was increased to 300cc. This operation was completed in two minutes (total 10 minutes); the starch solution was then homogenised in a homogeniser for 5 minutes at 16000 R.P.M. Then solution was transferred to a 500cc measuring flask and volume was made upto 500cc. The pH of this starch solution was 11.

5.3.3.2 Modified Causticized Method

In this method the same procedure given above was repeated except the homogenisation part. This resulting solution was transferred to a 500cc measuring flask and volume was made upto 500cc. The pH of this starch solution was 11.

5.3.3.3 Preparation of Poly Acrylamide[22]

The poly acrylamide can be prepared by the following method:

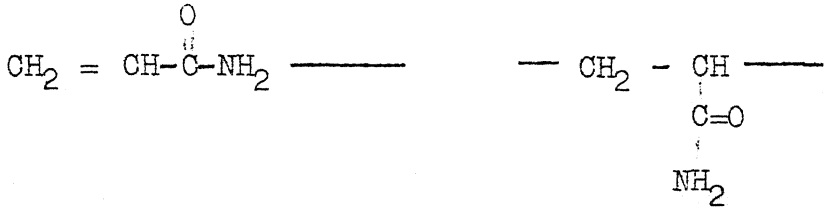

In a three method flask equipped with stirrer gas inlet, thermometer and condensor were placed 51.8 acrylamide and 414.7g distilled water. The acrylamide solution was stirred and heated to 68°C under a rapid stream carbon-dioxide. Then 7.7g Isopropyl alcohol and 0.069g pottassium per sulphate were added. The temperature of the reaction rises to 75-80°C where it was maintained by a heating bath for 2 hrs. The product was obtained in clear, colorless solution having high viscosity. The polymer can be precipitated in methanol, washed well with methanol and dried in a vacuum at 50°C. The inherent viscosity was about 1.0 (1N solution of

sodium nitrate 0.5 polymer concentration 50°C). The relationship of intrinsic viscosity to molecular wt was

$$= 3.73 \times 10^4 M^{0.66}$$

where M is the weight average molecular wt.

The product was stored in methanol. The molecular wt. varies with the initiator concentration as follows:

$$M \propto \frac{1}{\sqrt{c}}$$

where M = Molecular weight and

c = Concentration of initiator

5.3.3.4 Preparation Method of Poly Acrylic Acid

Solution of 10 grams (~ 0.14 mole) of acrylic acid and 0.1gm (0.0004 mole) of benzoyl peroxide dissolved in 30 gm of toluene was heated. At the boiling point of the solvent a very violent reaction takes place. Heating is discontinued. After 15 minutes the reaction mixture is cooled and the product a volumenous white powder is isolated by filtration. After drying at reduced the yield is ~ 9 gm (90% yield). The product is said to be water soluble.

5.3.3.5 Preparation Method of Xanthate Introduced Poly Acrylyamide

100 ml of acrylamide (0.5% aq. solution), 1.7 ml CS_2, 6.7 ml of formaldehyde and 1.0 gram of NaOH were heated at 40°C for approximately 1/2 - 1 hrs until the solution turns yellow orange in colour.

The shelf life is only 24 hrs so it has to be used before it decomposes.

5.3.3.6 Preparation of Amylo Pectin

The required quantity of amylopectin powder was made into a paste with water and dissolved in boiling water. The resulting solution was again boiled for 5 minutes. The resulting solution was made upto the desired volume to achieve the concentration.

5.3.4 Acid Analysis

The given amount of ore material was dissolved in minimum amount of concentration hydrochloric acid and digested for 7-8 hrs at 60°C. The resulting solution was filtered and dried and weighed.

Acid solubility = 100 - % of weight remaining.

5.3.5 Apparatus Used

A : This apparatus has 3 cm dia, 16.5 cm high cylindrical jar in which the height of 100 cm^3 pulp was 11.5 cm, and the sampling port height from the base 3.5 cm.

B : This flocculating column is of 11 cm internal diameter and 24.5 cm height. The tapping port was at a distance of 19.5 cm from the top of the flocculating column. Suspensions of two pure minerals were mixed to constitute the total pulp of 1600 cm^3.

C : This flocculating column is of 63 cm. height in the cylindrical portion 12 cm internal diameter with a conical bottom. In the cylindrical portion, there were 3 taps T_1, T_2 and T_3 at heights of 41 cm, 21 cm, 7.5 cm respectively, from the base of the cylindrical portion, and the conical part fitted with tap T_4. The central shaft was fitted with a stirrer at the base of the cylindrical part. For one experiment, an additional stirrer was fixed on the shaft .53 cm above the bottom stirrer. The capacity is 12 litres.

The following beneficiation studies were carried out in this work:

(1) Magnetic separation

(2) Selective flocculation

(3) Settling studies.

5.4 Magnetic Separation

It was clear from the x-ray diffraction pattern of different coloured particle (Fig.3.3) that almost all the dark coloured particle contain magnetite which is strongly ferromagnetic in nature. It was also seen from the petrological results that -100 mesh materials are fairly liberated. This work on magnetic separation with available magnetic separation at IIT Kanpur exploited the above results to beneficiate the spiral tail material.

The magnetic and nonmagnetic fractions are sieve analysed and the results are tabulated in Table 5B.

This work was extended with another magnetic separator called Frantz Isodynamic Separator Model L-1 available in Geology Laboratory at IIT Kanpur. The apparatus has got a limitation that it can not receive material above 35 mesh. So the material was sieved with 35 mesh and was subjected to this separator at a side slope 15°, magnet slope 30° and intensity 0.0 to 0.10 amp. Another reason for sieving the material instead of grinding was that the coarse materials

were found to be rich in Iron Content. The material above 35 mesh was not less than 20% of the total feed. The results are tabulated in Table 5C.

5.5 Settling Studies

Some settling studies were also carried out with 0-74μ particle size. The studies were done by dispersing the material with various concentration of dispersents and at various pH. The conditioning time was 10 minutes during which the pH was stabilised to the desired value. The experiment was done in the same 16.5 cm high settling column with settling time 5 minutes and 30 sec. This settling time was selected to settle the particle below 10 . The pH worked was 7.2, 9.2, 11.2 and flocculant concentration was 0 ppm, 20 ppm, 40 ppm and 80 ppm. The results are tabulated in Table 5D, and their behaviour is depicted (Fig.5.1).

Some preferential settling experiments were done in the apparatus described with starvation dosage (very low concentration) of starch.

5.5.1 A sample of 150g lot of non-magnetic portion of spiral tail was mixed and stirred with a 12 litre of water and dispersant for 10 minutes in flocculating column (C). Then the stirrer was stopped and one minutes settling time was allowed. Fractions were collected through T_1, T_2, T_3

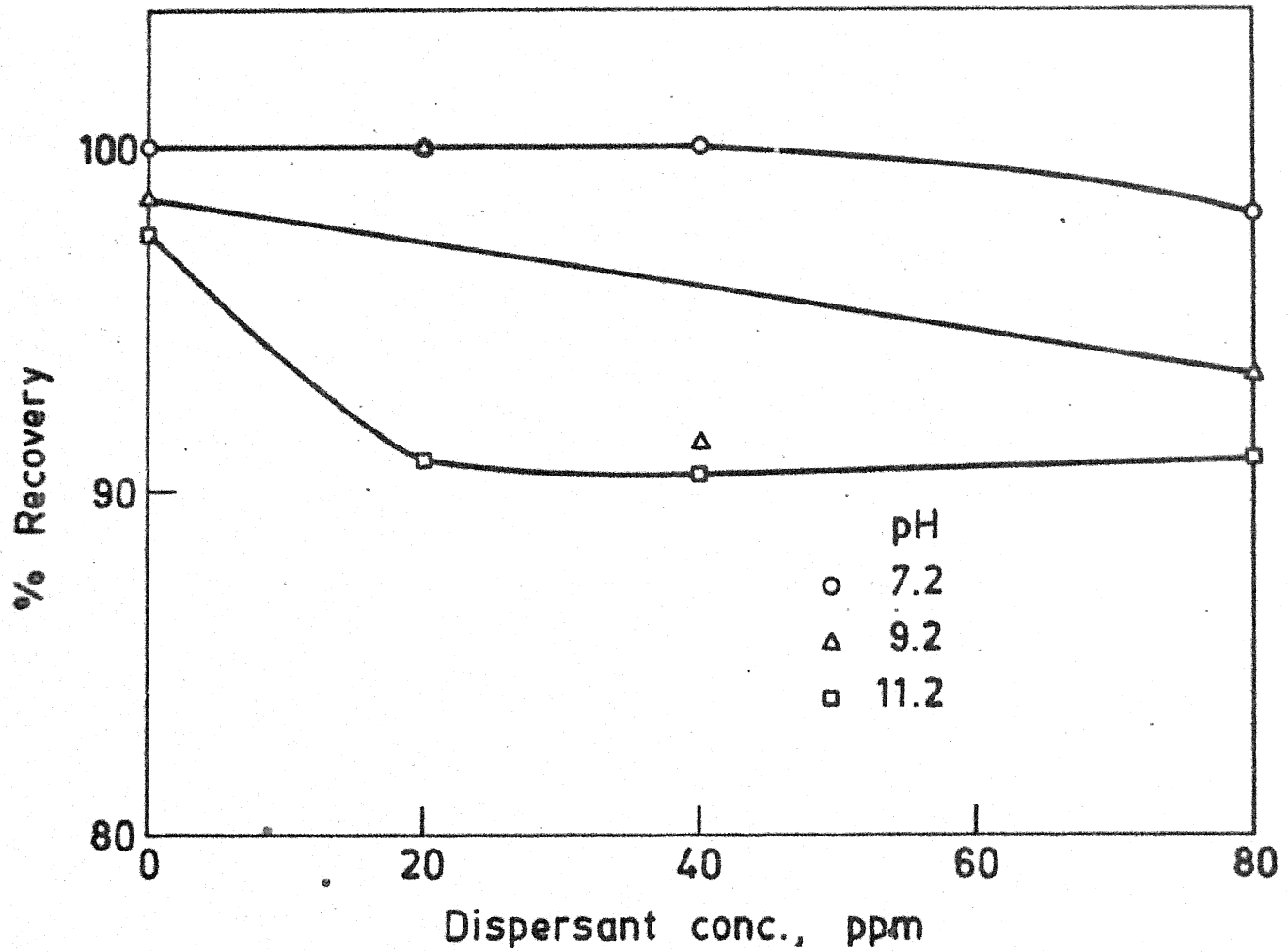

Fig. 5.1. Effect of pH and dispersant concentration on recovery, 0 - 74 μ particle system.

and T_4 in succession T_4 collecting the most quickly settling heavy fractions. The solid content in these fractions were allowed to settle for about a day or so, the supernatent liquid was decanted, the remaining solid slurry was dried, weighed and chemically analysed. This experiment was done at the pH attained by the whole liquid (i.e. at 6.9. The results are tabulated in Table 5E.

Two stage selective settling experiments were performed with the spiral tail material as such. The dispersant was used in each stage corresponding to the depletion in concentration. This was performed in a flocculating column of 11 cm internal diameter and 24.5 cm height. The tapping port was at a distance of 19.5 cm from the top of the flocculating column. The total pulp was made up to 1600 cm^3. The conditioning time used was 3 minutes and settling time was 1 minute. The pH attained by the system after the addition of dispersant water etc. was taken as the working pH. The results are given in Table 5F.

This settling experiment gave the grade very much nearer 10 the grade obtained after IInd stage. The reason may be due to the desliming action took place at the first stage which was absent in the subsequent stage.

5.6 Flocculation Studies

Since the liberation is fairly good enough below 400 mesh and also considering the problem of fines selective flocculation methods were tried with various flocculants.

Some spot experiments on pure minerals magnetite, hematite, quartz and ore system were performed on 0-74μ to optimize the parameters like settling time, dispersant concentrations to some extent.

It was found out that 1 minute settling time and 40 to 80 ppm of sodium silicate concentration would be optimum for the one system. With this back ground the flocculation work on laboratory model column (A) was performed.

5.6.1 Effect of Flocculant Concentration on Recovery at Different pH

This work was performed to optimize the pH and flocculant concentration. The work was carried out in small flocculation column (A) with a port at the bottom. The apparatus description was given already. The conditioning time allowed in this experiment after adding dispersant and flocculant was 3 minutes. The settling time was 1 minute. During conditioning the slurry was given some agitation. The flocculant used was modified and causticized starch. The results are tabulated in the Table 5G and shown in Fig.5.3. Their reproducibility was also checked.

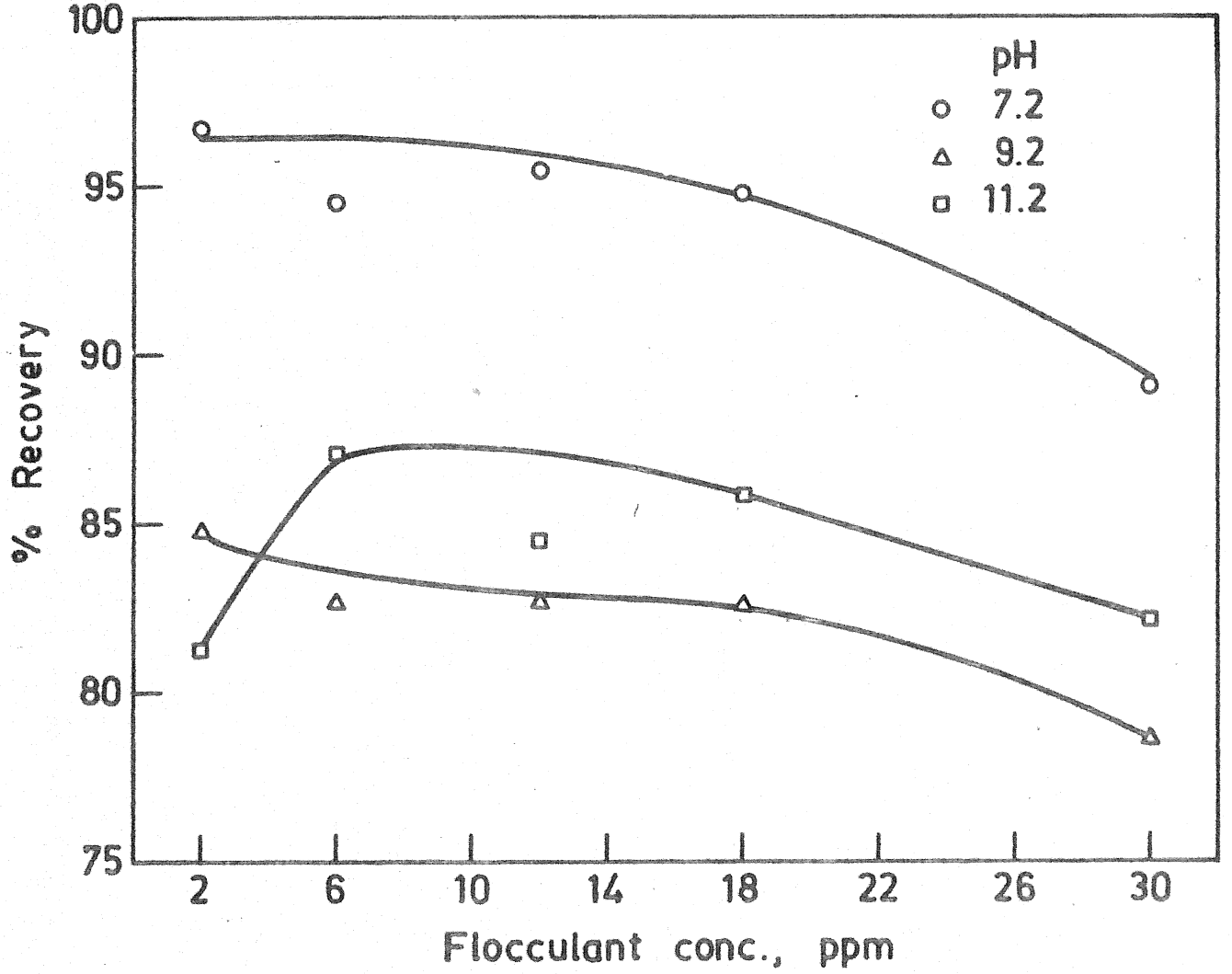

Fig. 5.2. Effect of flocculant (modified caustisized starch) concentration on recovery at constant concentration, 40 ppm.

5.6.2 Effect of Modified Causticized and Homogenised Starch on (0-72 μ) Ore System

The experimental procedure is very much similar to the above one. The results are tabulated in Table 5H and shown in Fig.5.3.

5.6.3 Effect of Different Flocculants on Recovery at Higher pH

The experimental procedure was very much similar to the earlier ones. The working pH was 11. The different polymers used were amylopectin, polyacrylamide and zanthate introduced polymer. One desliming experiment at 11.2 pH was also carried out and the washings were done for 3 times. The results were tabulated in Table 5I and the behaviour was represented in the Fig.5.4.

The above experiments results insticated the idea of reducing the particle size to 0-20 μ from 0-72 μ in the previous cases. The experimental procedure was quite similar to the earlier ones. The working pH was not made alkaline. It was 6.9. The results are tabulated in Table 5J and behaviour of each flocculants are shown in Figs.5.3A, 5.3B. The flocculants used were modified causticized, amylopectin, xanthate introduced polymer, polyacrylamide of high, middle and low molecular weight (relative).

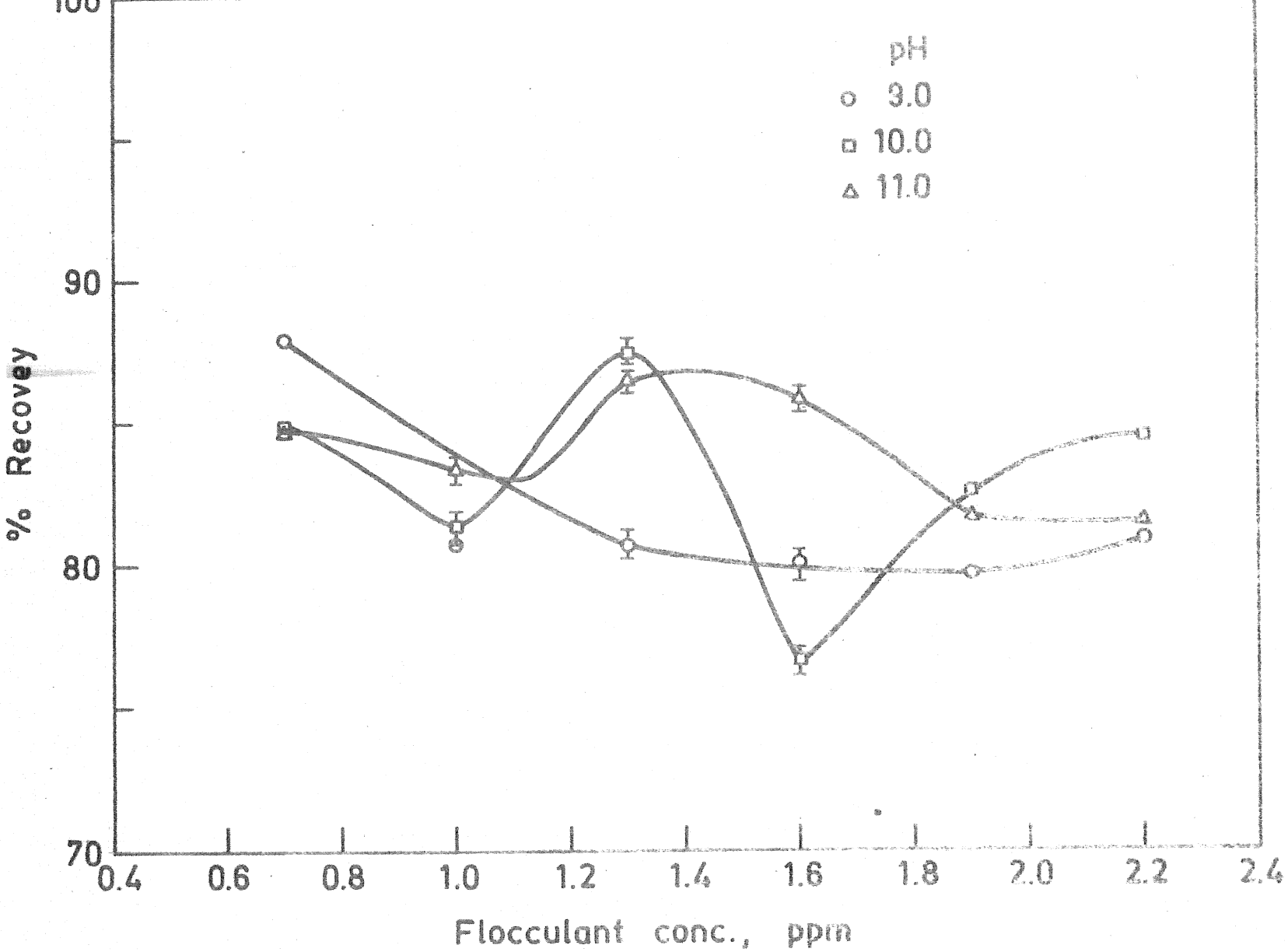

Fig. 5.3. Effect of flocculant (modified caustisized homogenized starch) concentration on recovery at dispersant concentration, 50 ppm.

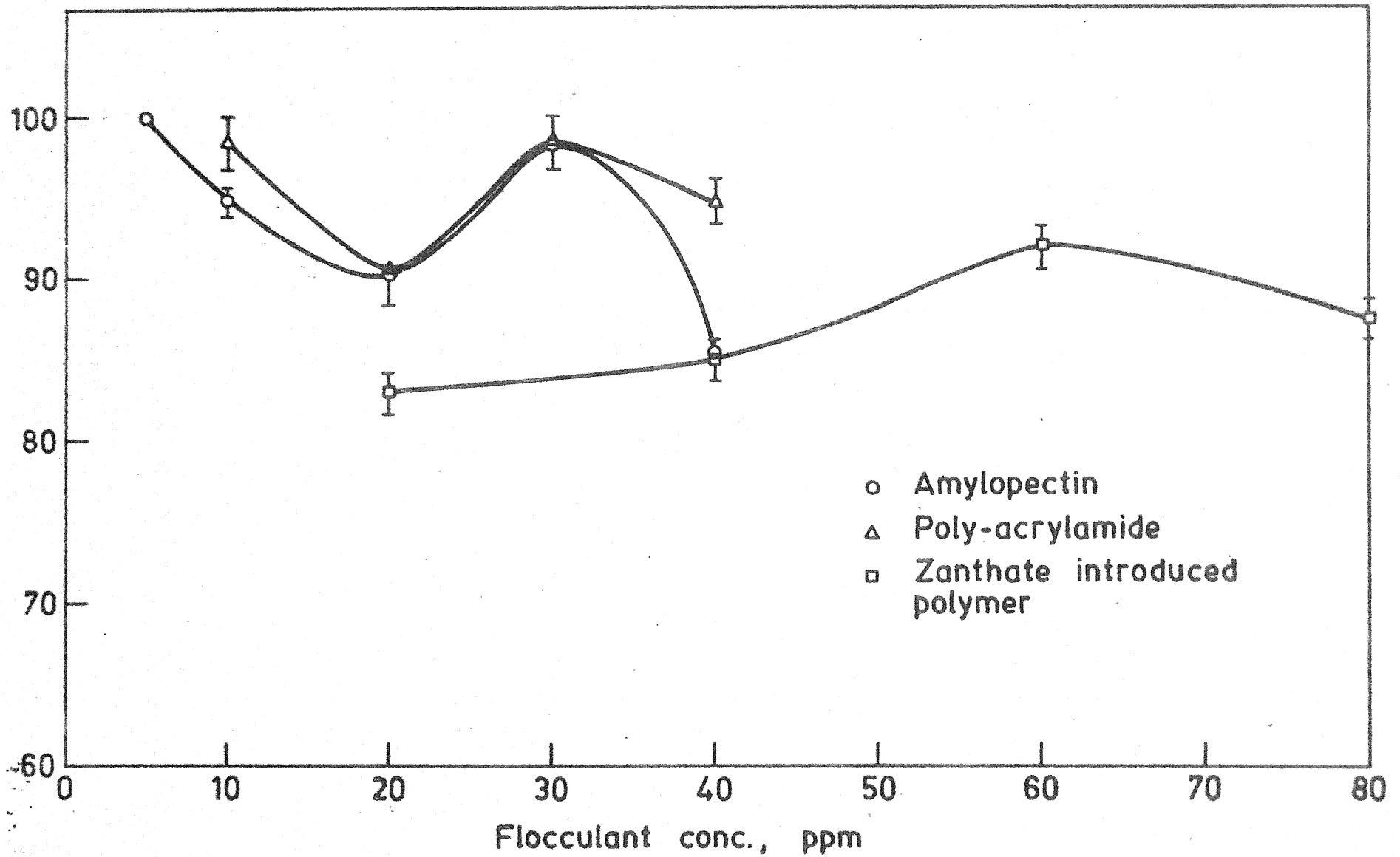

Fig. 5.4. Effect of various flocculants on recovery of the tail at pH 11.

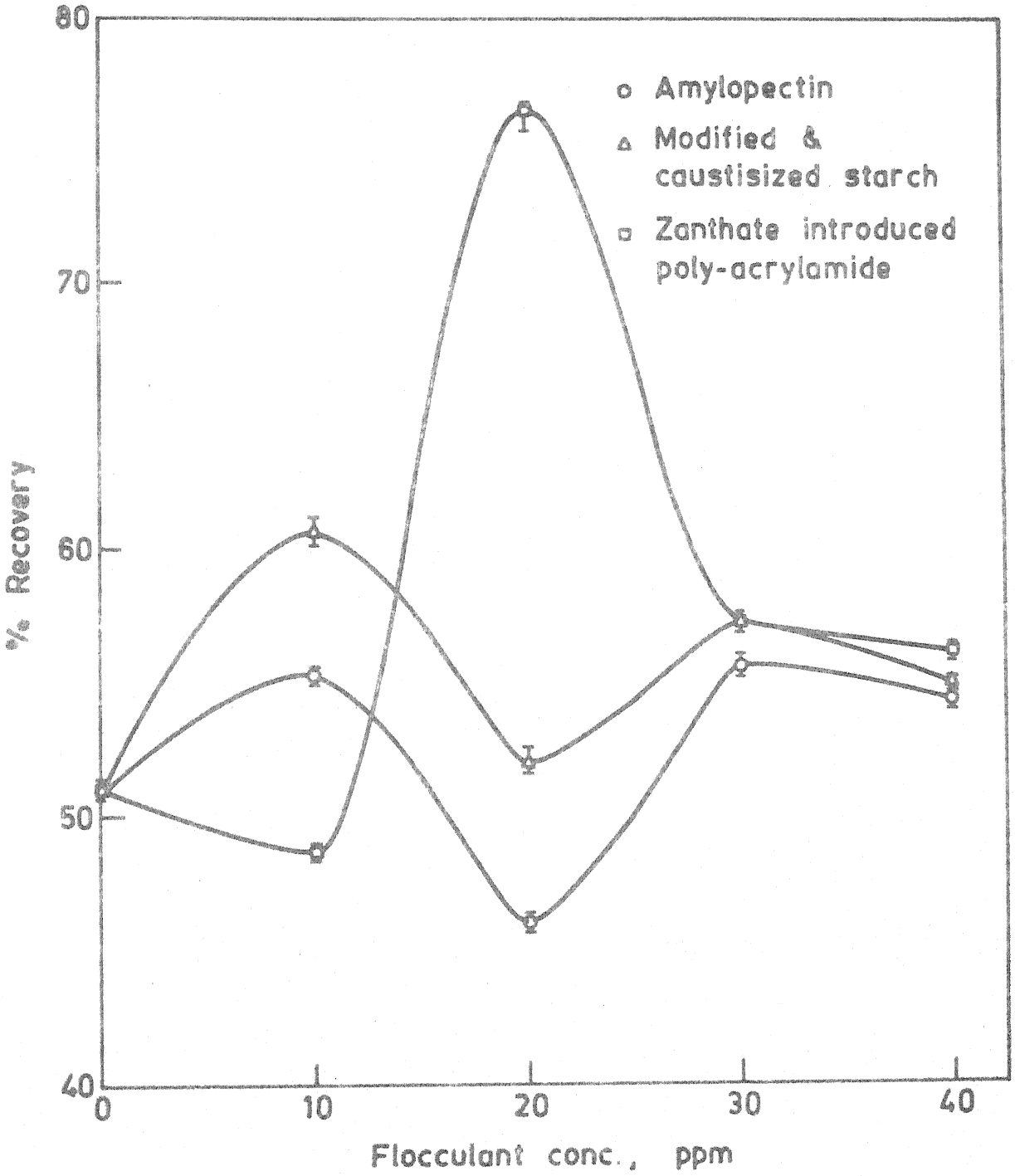

Fig 5.5a Effcect of flocculant concentration on recovery at constant dispersant concentration at pH 6.9

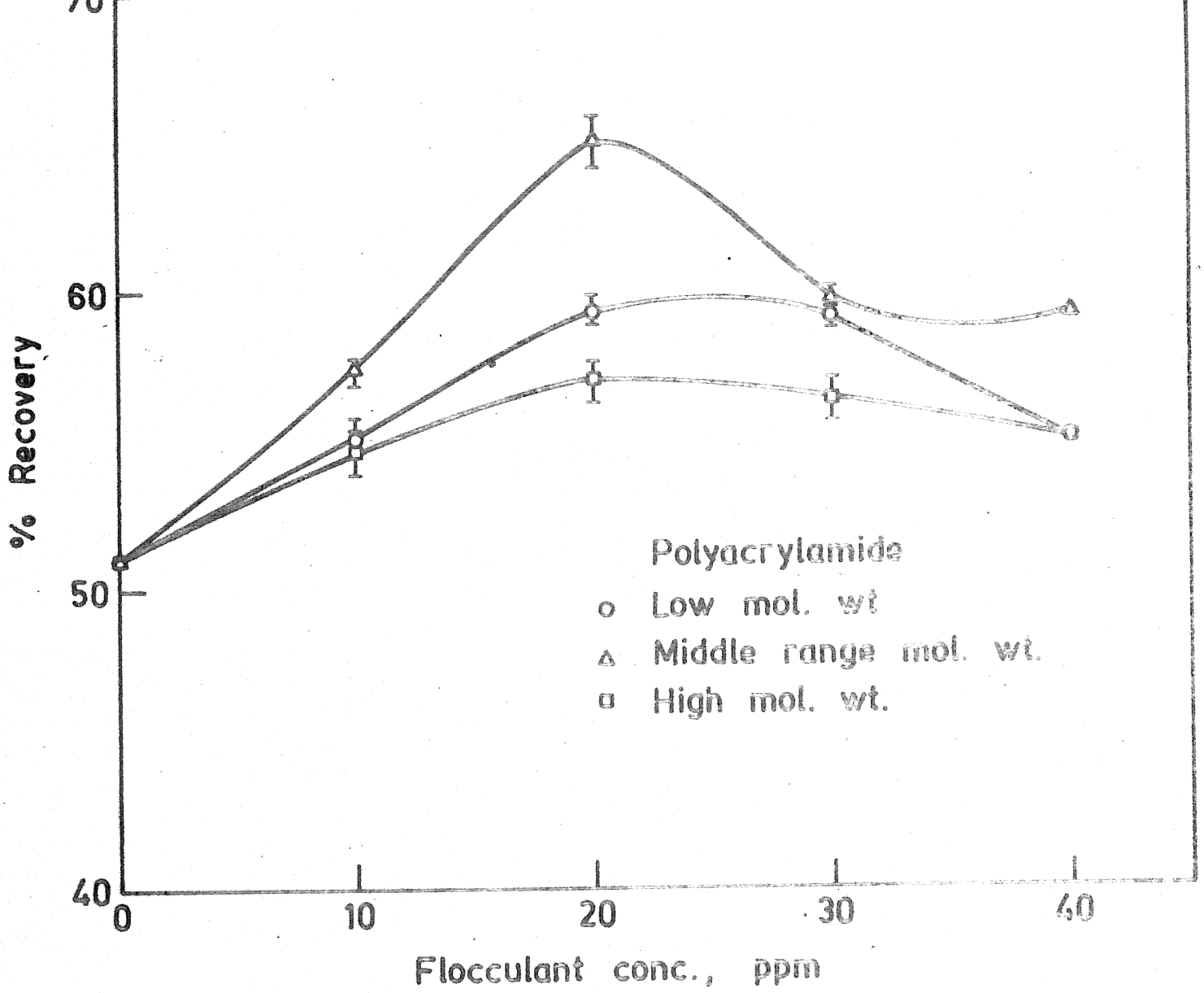

Fig. 5.5b. Effect of flocculant concentration on recovery at constant dispersant concentration, 50 ppm.

5.6.4 2-Stage Selective Flocculation Experiment

With the best of the results, obtained from the above experiment, repeated flocculation studies are carried out. The experimental procedure was quite same as in the previous cases and was repeated twice to complete 2-stages. The results were given in Table 5K.

Some more flocculation experiments were done on the spiral tail as received but they were not successful due to the wide particle size range.

Flotation experiments tried with spiral tail as received and nonmagnetic fraction of spiral tail -150 mesh with dodecyl amine as the collector. But it was found that this collector was floating the black particles which are essentially iron bearing minerals.

CHAPTER 6

RESULTS AND DISCUSSION

6.1 Characterisation Studies

This thesis outlines the results of investigations of (1) liberation and (2) characterisation studies. The research efforts include optical microscope, x-ray and transmission electron microscopy. Liberation studies on various size particles revealed that the materials $< 147\mu$ (-100 mesh) are liberated enough to enter into any venture of further beneficiation.

The results obtained from the polished mounted typical representative samples of spiral tail showed that the minimum size of the particle locked in the matrix was about 6.5μ . The results are substantiated in Fig.2.3 . X-ray diffraction pattern of typical particles picked up from the spiral tail confirmed that the black particles consists of magnetite, hematite, maghemite and goethite. As the colour becomes lighter the presence of Iron bearing mineral also decreases. The white particles are found to be mainly quartz. The results of micro hardness values also show that as the colour darkens the micro hardness value decreases. The value ranged from 200 kg/mm^2 to 15 kg/mm^2 in Vicar's scale from white particles to black particles.

These phases are highly intermixed still some information about the grain size was procured by etching the sample by HF. The average grain size of typical black and red particles are 25μ and 10 μ respectively. The grain size of quartz is very fine and is unresoluable by ordinary optical microscope.

Phase identification work was carried out on different samples subjected to different treatment by XRD Technique and the final results are as follows. The phases present are Magnetite, Fe_3O_4; Hematite, Fe_2O_3; Maghemite (C), γ-Fe_2O_3; Maghemite (T), γ-Fe_2O_3; Goethite, $Fe_2O_3H_2O$; Quartz, SiO_2; Grunerite, $(Fe_{0.7}Mg_{0.1})(OH)_2Si_8O_{22}$ Tremolite, $Ca_2Mg_5Si_8O_{22}(OH)_2$; Kirschsteinite, Ca $FeSiO_4$; Vermiculate, $(Mg_{2.37}Fe_{0.37}X_{0.36})(Al_{1.28}Si_{2.72})O_9(OH)_3\ 4H_2O$; Vivianite, $Fe_3(PO_4)_2\ 8H_2O$; Alunite (KNa) $Al_3(OH)_6(SO_4)_2$, Iron Silicate (M), $FeSiO_3$; Iron Silicate (OR), $FeSiO_3$; Kyanite, Al_2SiO_5; Chlorite $(Mg_{2.6}Fe_{2.2}Al_{1.2})Si_{2.8}Al_{1.2}O_{10}(OH)_8$; Collinsite, Ca_2 (Mg.Fe) $(PO4)_2\ 2H_2O$; Akaganite, FeOOH Lepidocrocite, FeO(OH); Gibbsite, $Al(OH)_3$; Pyrolusite, MnO; Siderite, $FeO.CO_2$; Calcium Aluminum Silicate, Ca Al_2SiO_6;

Some of these phases have been confirmed by electron diffraction pattern.

They are as follows:

quartz, SiO_2; Alunite, (k.Na)$Al_3(OH)_6(SO4)_2$; Maghemite (T), -Fe_2O_3; Pyrite, FeS_2; Magnetite, Fe_3O_4;

$CaAl_2SiO_6$; Iron Silicate (OR), $FeSiO_3$; Wustite, FeO; Maghemite (C), γ -Fe_2O_3;

The major Iron bearing minerals are Magnetite, Hematite, Maghemite (T) and Goethite to some extent. The major gangue mineral is quartz. According to the chemical analysis in the Chapter 5, some of the phases can be eliminated. The CaO + MgO content is only 0.024% so it is likely that some of the Magnesium and Calcium bearing minerals may not be present. But it is difficult to predict explicitly which of those may not be present.

Besides, the already reported phases by the earlier workers, a few new phases have also been identified and some of them are confirmed* by TEM.

These phases are (1) Maghemite (C)*, γ -Fe_2O_3; (2) Maghemite* (T), γ -Fe_2O_3; (3) Lepidocrocite, α-FeO(OH); (4) Akaganite*, β- FeOOH; (5) Calcium Aluminum Silicate*, $CaAl_2SiO_6$; (6) Alunite* (kNa) Al_3 $(OH)_6$ $(SO4)_2$; (7) Kyanite Al_2SiO_5; (8) Collinsite, $Ca_2(MgFe)(PO4)_2 2H_2O$; (9) Wustite*, FeO;

---

* Represents the confirmed phases by TEM.

6.2 Beneficiation Studies

These liberation and characterisation works encouraged to beneficiation studies. These works were initiated by magnetic separation. The experiments conducted by laboratory magnetic separator gave 3.5% of magnetic fraction of grade (Fe_2O_3) 98.2%. The coarse material (+48 mesh, 30% of the total spiral tail material assaying 80%) and the fine material (-325 mesh 5% of the total spiral tail material assaying 88%) are found to be rich in valuable minerals. The recovery is also found to be (44%) in +48 mesh material. Improved results are obtained when the material was subjected to Frantz Isodynamic separator which gave 3.3% of total material assaying 98.1% and the recovery is 6.09%. Due to the constraint in the apparatus only -35 mesh material was fed into the hopper. But the material above 35 mesh gave a grade which is at par excellence with that of the grade obtained by selective flocculation experiment. This result can also be extended in terms of further grinding and magnetic separation to achieve a good grade.

Though this magnetic separation process gives 7-8% of the concentrate (Assay 99%), it is not a negligible amount in the total of 12.5mtpy.

Selective flocculation appeared to be a promising technique of beneficiation and was able to beneficiate the spiral tail material from 48.1% acid solubility to 81%

acid solubility. Flocculation experiments performed on three size ranges of particle, viz. (1) on spiral tail as received (2) on 0-74 μ* of the spiral tail and (3) on 0-20 μ particle size distribution.

In the first case the flocculation did not help at all. For the simple reason that the size range is too wide to be used for flocculation. In the second case the flocculation experiments with modified causticized polymers at higher pH around 11 gave the highest acid solubility in that set of experiments (ie) 54.27% solubility with 87% recovery gave selectivity Index 1.78. The value was attained at a much lower flocculant concentration. The poor grade may be due to the coiling of flocculant at such a high pH. Moreover this flocculant was not homogenised before use. The homogenisation causes breaking of longer chains into shorter ones which enable the flocculant to adsorb more easily without steric hinderance.

The flocculation experiment was carried out using modified causticized and homogenised starch. The results showed 57% assay Fe_2O_3, 87% recovery in a few cases at the pH 10 and 11 and at low concentrations of flocculant (say 5 ppm and 20 ppm). The selectivity index is 2.074. There is a dip at 10 ppm almost in all the pH values taken for the experiment.

---

* Note: This material used for flocculation is the non-magnetic fraction of spiral tail.

One more set of flocculation experiments were tried with the same particle system 0-74 μ with different polymers like A amylopectin, polyacrylamide and xanthate introduced polyacrylamide. A good result of this set of experiments is (i.e.) 59% assay (Fe_2O_3) and more than 95% recovery in all the 3 polymers (i.e.) in amylopectin, polyacrylamide and xanthate introduced polyacrylamide at 30 ppm, 40 ppm and 40 ppm respectively. The selectivity indexes are 5.74, 3.09 and 1.9226. The behaviour of the curve is quite the same as that of the last set of experiments. From the above results it is expected that had the particle size been reduced from 0-74μ to 0-20 μ by further grinding the flocculability could have been improved significantly. The experiments performed in this size range are with polymers modified causticized, amylopectin, xanthate introduced polyacrylamide, polyacrylamide of low, medium and high molecular weight. The assay (Fe_2O_3) improved a little bit the recovery fell down compared to the previous case. The best result of this set was obtained with xanthate introduced polymer (i.e.) 78% acid solubility and 76.50% recovery with selectivity index 3.625 at 20 ppm flocculant concentrations unlike the previous case where it was 56% assay (Fe_2O_3) and 82% recovery. Polyacrylamides are also at par excellence with amylopectin. Modified causticized has performed well at higher concentration, 40 ppm, which gave an assay (Fe_2O_3) 71% and recovery 55%.

Some two stage flocculation experiments were performed with the best of the results got in the previous case, showed that the assay (Fe_2O_3) can be improved 3% more (i.e.) to 81% at the expense of the recovery.

Settling experiments were done to check the chance for gravity separation or jig. The Ist set of experimental results in settling experiments (Table 4(i)) show that suspension stability was comparatively better at higher pH and higher concentration of dispersant, say, 80 ppm.

The second set of experiments performed in this line with starvation dosage of flocculant (2 ppm) showed that by more settling itself it is possible to get 66% assay (Fe_2O_3) and 71% recovery at 100 ppm dispersant concentration. The suspension stability at this concentration of dispersant is quite good. So desliming action has helped significantly to achieve a better assay (Fe_2O_3). The experiment done at 1000 ppm dispersant concentration was found to be over dozed with dispersant and hence selective settling did not help much here. The experiment done at 10 ppm dispersant concentration gave inferior result due to inadequate dispersing action and hence selective settling. From the weight of the material settled in this case it is clear that the suspension stability is very poor to promote selective settling.

Settling experiments tried with spiral tail as received, did not give good result probably due to the poor experimental set up available at IIT Kanpur.

Comparing selective flocculation and settling experiments on 0-74 μ particle size range, the settling experiments have shown better performance than selective flocculation. Flotation experiments have turned out to be a failure because of the poor selectivity of the collector do decyl amine. It floated some black particles also along with quartz.

6.3 Conclusions and Suggestions

As far as the characterisation studies are concerned one can still explore as many minor phases as possible. The previous workers found that martite is one of the major iron bearing mineral other than hematite and magnetite. But in this it is found that it is maghemite and not martite. Another important gangue mineral found is calcium aluminium silicate. A detailed elemental analysis could have been possible if energy dispersive analyser (EDAX) had been available.

As far as the beneficiation work is concerned it is observed that even laboratory low intensity magnetic separators could separate some iron bearing mineral of high grade . Though the amount recovered is small around 5% of the total

material, it should be possible WHIMS to produce efficient separation both in grade and recovery point of view. In the actual beneficiation plant, improving the efficiency of the magnetic separators and increasing recycling would be one of the suggestions in this part.

Since there is an appreciable difference in the densities of the iron bearing minerals and gangue minerals one can think about the beneficiation by efficient jig or gravity separation.

Flotation can also be adopted since the liberation is good enough below -100 mesh. Since the amine floats both quartz and magnetite one has to think about a depressor which can prevent magnetite from floating or alternatively a more selective collector may be used.

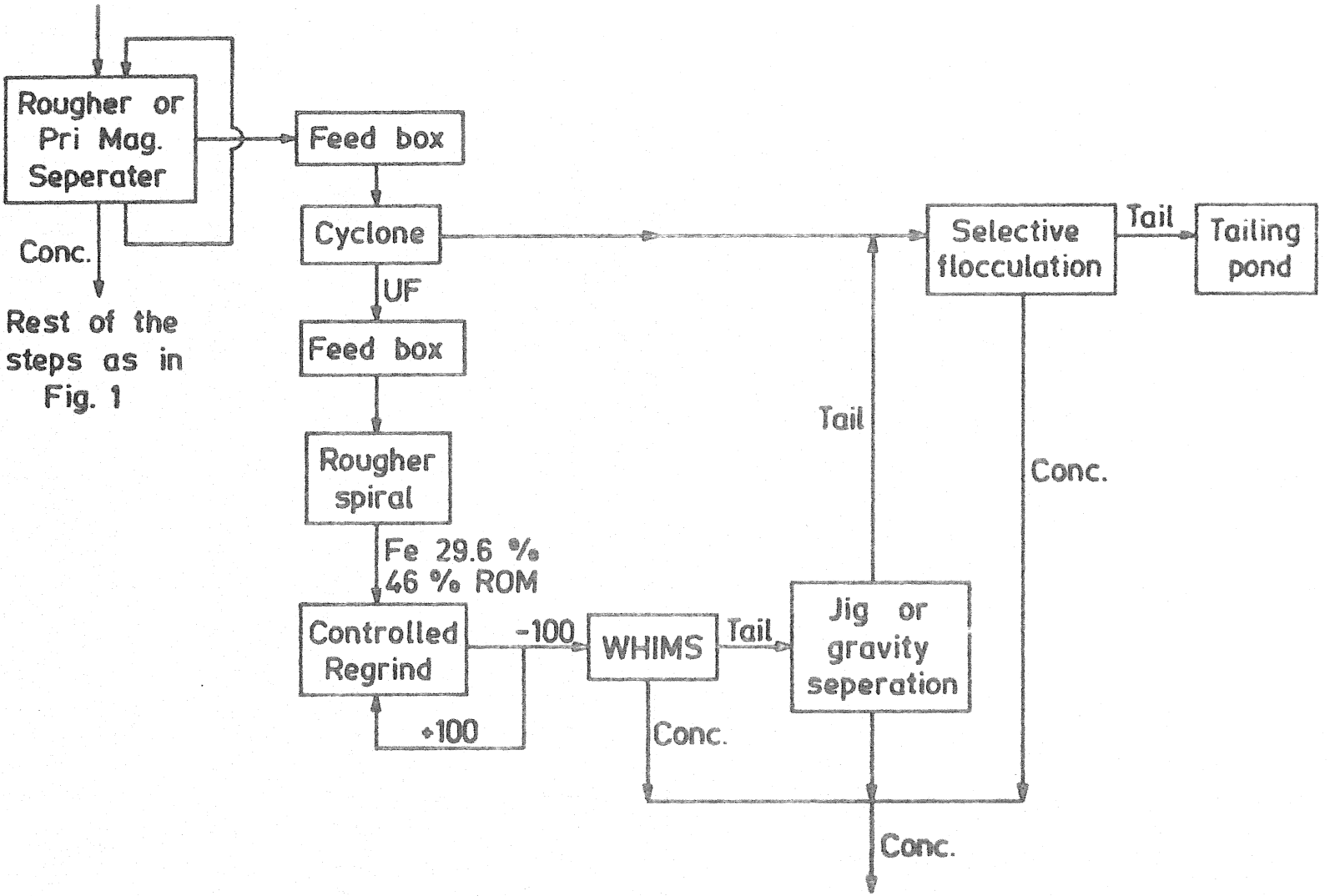

Fig. 6. Modified flow sheet.

REFERENCES

1. Viswanathan, S., and Paranjpe, Washing and Agglomeration if Iron Ores, Trans. Indian Inst. of Metals, 21, 2, 71, 1968.

2. Narayanan, P.I.A., and Ramakrishna Rao, G.S., Beneficiation of Indian Iron Ore and Allied Problems, Trans. Indian Inst. of Metals, 21, 2, 79, 1968.

3. Irani, J.J., and Viswanathan, S., Considerations on Sizing of Blast Furnace Raw Materials, TISCO Journal, pp.119-126, Oct. 1971.

4. Sen, P., and Misra, D.D., The Problem of the Iron Ore Fines in India, NML Technical Journal, 14, 47-55, May 1972.

5. Kelly, G.E., Spottiswood, J.D., Introduction to Mineral Processing.

6. Lawver, J.E., and Hopstock, D.M., "Wet Magnetic Separation of Weakly Magnetic Minerals, Miner. Sci. Eng., 6, pp.154-172 (1974).

7. Jones, G.H., "Wet Magnetic Separator for Feebly Magnetic Minerals: Description and Theory", Proc. 5th Int. Miner. Process Congr., London, 1960, pp.717-732 IMM (1960).

8. Jannicelli, J., New Developments in Magnetic Separation IEEE Trans. Magn. MAG. 12, pp.436-443 (1976).

9. Read, A.D., and Hollick, C.T., Selective Flocculation Techniques for Recovery of Fine Particles Mineral Sci., Engng. Vol. 8, No.3, July 1976.

10. Sresty, G.C., and Somasundaran, P., Beneficiation of Mineral Slimes Using Modified Polymers as Selective Flocculants, XII IMPC, Sao Paulo, Brazil, 1977.

11. Sresty, G.C., Raja, A., and Somasundaran, P., Selective Flocculation of Mineral Slimes Using Polymers. Recent Advances in Separation Science, Vol. IV, CRC Press, 1978.

12. Read, A.D., Selective Flocculation Separations Involving Hematite, Trans. of the Institution of Mining and Metallurgy Section C, Vol. 80, 1971, C24.

13. Frommer, D.W., Preparation of Nonmagnetic Taconites for Flotation by Selective Flocculation, Prox. XIth Int. Mnl. Proc. Congr. Cagliari, Paper D-9, 1975.

14. Dicks, MasoulL, Morrow, J.B., Application of the Selective Flocculation-Silica Flotation Process to the Mesabi Range Ore. Paper presented at 1978 AIME Annual Meeting Denver, Colorado - Feb. 28 - March 2, 1978.

15. Iwasaki, I., Carlson, W.J., and Parameter, S.M., The Use of Starches and Starch Derivatives as Depressants and Flocculants in Iron Ore Beneficiation, Paper presented at Annual Meeting of AIME, 1969.

16. Gururaj, B., Prasad, N., Ramachandran, T.R., and Biswas, A.K., Studies on Composition and Beneficiation of A Fine-Grained Alumina-Rich Indian Iron Ore XIII IMPC, Warsaw, Poland June 4-9, 1979 Proceedings, 16/IMPC, Paper No.8, pp.154-182.

17. Sisselman, R., Cleveland - Cliffs takes the wraps off Revolutionary New Tilden Iron Ore Processes, New Tilden Iron Ore Process Engg. and Min., J. 176 (10), 79, 1975.

18. Guccione, E., New Process Unlocks Tilden's Huge Ore Reserves, Min. Engg., 27(11), 21, 1975.

19. Paananen, A.D., and Turcotte, W.A.,"Factors Influencing Selective Flocculation - Desliming Practice and the Tilden Mine", Paper presented at AIME Meeting, Feb. 1978.

20. Arthur, F. Colombo, Paper presented in the Symposium on Fine Particles Processing, 1978.

21. Krishnan, S.V., and Iwasaki, I., 1984 Pulp Dispersion in Selective Desliming of Iron Ore, Int. J. Miner. Process., 12 : 1-13, 1984.

22. Cabaness, W.R., Yenchunlin, T., and Parkanyi, C., J. Polymer Sci., 9 (1971) pp.2155-170.

APPENDIX A

Standard error on the regression co-efficient (slope)

$$= \frac{S_{yx}}{\sqrt{x_1^2 - \frac{(\bar{x}_1)^2}{n}}}$$

where $S_{yx} = \sqrt{\frac{\Sigma(y-y_1)^2}{n-2}}$ where n = sample number = 8.

Here R is plotted along y axis and $\sqrt{h^2+k^2+l^2}$ along x-axis.

The slope has been found to be 0.6445

$$\bar{x} = \frac{22.172}{8} = 2.77125$$

$$\bar{y} = \frac{14.14}{8} = 1.7675$$

So the equation of the line is

$$y - \bar{y} = b\,(x - \bar{x})$$

$$y - 1.7675 = 0.6445\,(x - 2.77125)$$

$$y = 0.6445\,x - 0.0185706$$

$x_{measured}$	$y_{calculated}$	$y_{measured}$	$(y_{measured} - y_{calculated})^2$
0	-0.0185706	0	3.44867×10^{-4}
1.732	1.0977034	1.09	5.93423×10^{-5}
2	1.2704294	1.20	$1.08772 \times 10^{-+}$
2.828	1.8040754	1.80	1.65088×10^{-5}
3.317	2.1192359	2.10	3.70019×10^{-4}
3.464	2.2139774	2.20	1.95367×10^{-4}
4.359	2.17908049	2.79	6.47864×10^{-7}
4.47	2.8636334	2.9	1.32252×10^{-3}

$$\leq = 2.41813 \times 10^{-3}$$

$$\therefore S_{yx} = \frac{2.41813 \times 10^{-3}}{8-2} = 0.0200753$$

$$\therefore \sqrt{x_1^2 - \frac{(x_1)^2}{n}} = \sqrt{77 - \frac{(22.172)^2}{8}} = 3.9433872$$

Hence standard error in slope $= \frac{0.0200753}{3.9433872} = 5.09 \times 1 =^{-3}$

$$\text{Slope} = \frac{L\lambda}{a}$$

$$L\lambda = \text{slope} \times 4.0783$$

Hence error in $L\lambda$ value $= 5.09 \times 10^{-3} \times 4.0783$

$$\text{pct error in } L\lambda \text{ value} = \frac{5.09 \times 10^{-3} \times 4.0783}{2.63}$$

$$= 0.789 \text{ pct.}$$

APPENDIX B

The selectivity index was calculated as defined by the text by the following formula:

$$\text{Selectivity Index} = \sqrt{\frac{R_{vm}}{(100-R_{vm})} \quad \frac{R_{lvm}}{(100-R_{lvm})}}$$

APPENDIX C

SAMPLE CRUDE ORE

Table 3A

2θ	Relative Intensity	dA°	Compounds with corresponding d value mA° and planes
20.8	12	4.267	Silica (4.26), 100 , Vermiculate 4.25 (022 or 112)
21.3	8	4.180	(1)γ -Fe_2O_3 Maghemite (C) 4.18 (200) (2) Grunerite 4.16 (220) (3) Tremolite 4.20 (220) (4) Goethite 4.18 (110)
24.2	8	3.6746	Hematite 3.66 (012) Kirschsteinite 3.672 (111)
26.6	100	3.34	Vivianite 3.33 ($\bar{2}21$) Quartz 3.343 (101) Alunite 3.34 $FeSiO_3$ (M) 3.35 (021) $FeSiO_3$ (OR) 3.34 (121) Kyanite 3.35 (200)
33.3	20	2.696	Hematite 2.69 (104) Goethite 2.69 (130) Kyanite 2.694 ($21\bar{1}$) Tremolite 2.705 (151) Vivianite 2.71 (041) Kirschsteinite 2.687 (131) Chlorite 2.68 ($20\bar{1}$) Collinsite 2.69 ($\bar{1}21$,$1\bar{2}1$)

35,4	8	2.53	Magnetite 2.532 (311) Collinsite 2.54 (012) Maghemite (T) 2.521 (119,313) Maghemite (C) 2.52 (311) Vermiculate 2.525 (202,20$\bar{4}$) Akaganite 2.543 (211) Vivianite 2.52 ($\bar{2}$41) Calcium Aluminum Silicate 2.535 ($\bar{2}$02, 002) Kyanite 2.52 (012, 11$\bar{2}$) Tremolite 2.529 ($\bar{2}$02,002) Goethite 2.52 (101)
35.7	12	2.51	Calcium Aluminum Silicate 2.509 ($\bar{1}$31) Hematite 2.51 (110) Goethite 2.49 (040) Fe-Silicate (OR) 2.51 (202,430) Grunerite 2.507 (20$\bar{2}$) Kyanite 2.509 (030)
36.7	12	2.45	Maghemite (T) 2.451 (305,314) Lepidocrocite (OR) 2.467 (031) Quartz 2.458 (110) Gibbsite 2.454 (021) Goethite 2.452 (111)
39.6	12	2.2733	Kyanite 2.272 (02$\bar{2}$, 12$\bar{2}$) Hematite 2.285 (006) Calcium Aluminum Silicate 2.27 (311) Tremolite 2.273 (112) Gibbsite 2.285 (31$\bar{2}$) Quartz 2.282 (102) Akaganite 2.285 (301) Vermiculate 2.265 (220,136) Chlorite 2.27 (20$\bar{4}$) Collinsite 2.25

40.4	6	2.23	Maghemite (T) 2.234 (316,219) Maghemite (C) 2.23 (321) Vivianite 2.23 Quartz 2.237 (111) Grunerite 2.225 ($31\bar{2}$) Gibbsite 2.244 (022,213) Kyanite 2.23 (300)
42.5	9	2.12	Fe-Silicate (OR) 2,134 (630,502) Quartz 2.128 (200) Pyrol .site 2.13 (111) Sidderite 2.13 (113) Collinsite 2.13 (030,$0\bar{3}1$)
43.2	8	2.09	Magnetite 2.0993 (400) Maghenite (T) 2.089 (400) Maghemite (C) 2.08 (400) Chlorite 2.10 ($20\bar{5}$) Vermiculate 2.08 (138) Lepidocrocite 2.09 (130,060) Akaganite 2.09 (321) Gibbsite 2.085 (114) Collinsite 2.40 ($1\bar{1}2,12\bar{2}$) Calcium Aluminum Silicate 2.090 (331)
44.8	8	2.0208	Tremolite 2.015 (202) $FeSiO_3$ (M) 2.039 (041) Vivianite 2.01 Vermiculate 2.01 (0014,208) Chlorite 2.01 (204) Maghemite (T) 2.01 (403,410)
45.8	6	1.98	Pyrolusite 1.98 (210) Fe-Silicate (OR) 1.995(440,241) Maghemite (T) 1.994 (412) Gibbsite 1.993 (023)

			Grunerite 1.996 (190,370) Quartz 1.98 (201) Vermiculate 1.975 (1.310) Collinsite 1.982
49.5	12	1.8394	Hematite 1.838 (024) Grunerite 1.837 (191,0.100) Lepidocrocite 1.848 (220) Kirschsteinite 1.835 (240,222) Maghemite (T) 1.835 (442) Collinsite 1.831 (031)
50.3	16	1.82	Maghemite 1.822 (T) (416,423) Pyrolusite 1.81 Vivianite 1.82 Quartz 1.817 (112) Tremolite 1.814 (530)
54.3	12	1.69	Hematite 1.69 (116) Goethite 1.694 (240) Tremolite 1.686 (003, 282) Gibbsite 1.689 (314) Grunerite 1.685 ($51\bar{2}$) Vermiculate 1.695 (314) Maghemite (T) 1.702 (426) Collinsite 1.695 (203)
55.1	6	1.6650	Calcium Aluminum Silicate 1.662 (313) Maghemite (T) 1.669 (500,409) Chlorite 1.67 (206) Vermiculate 1.665 ($20\bar{1}4$) Goethite 1.661 (060) Quartz 1.672 (202) Vivianite 1.67 Collinsite 1.669 ($\bar{1}13,\bar{1}40$)

57.0	6	1.6148	Kirschsteinite 1.610 (062,004) Maghemite (C) 1.61 (511,333) Magnetite 1.6158 (511)
60.0	15	1.5402	Calcium Aluminum Silicate 1.540 (600) Vermiculite 1.543 (2 0 14) Quartz 1.541 (211)
62.5	4	1.4845	Hematite 1.482 (300) Maghemite (C) 1.4810 (440) Magnetite 1.4845 (440)

TABLE 3B

SAMPLE CRUDE ORE

Phases	Number of times appeared
(1) Magnetite (Fe_3O_4)	4
(2) Hematite Fe_2O_3	7
(3) Maghemite (Cubic) γ-Fe_2O_3	6
(4) Maghemite (Tetragonal) γ-Fe_2O_3	9
(5) Goethite $Fe_2O_3H_2O$	7
(6) Quartz SiO_2	10
(7) Grunerite $(Fe_{0.7}Mg_{0.1})(OH)_2Si_8O_{22}$	6
(8) Tremolite $Ca_2Mg_5Si_8O_{22}(OH)_2$	7
(9) Kirschsteinite $CaFeSiO_4$	4
(10) Vermiculate $(Mg_{2.37}Fe_{0.37}X_{0.36})(Al_{1.28}Si_{2.72})O_9(OH)_34H_2O$	
(11) Vivianite $Fe_3(PO4)_2\ 8H_2O$	6
(12) Alunite (KNa) $Al_3(OH)_6(SO4)_2$	1
(13) Fe-Silicate (M) $FeSiO_3$	2
(14) $FeSiO_3$ (OR) $FeSiO_3$	3
(15) Kyanite Al_2SiO_5	6
(16) Chlorite $Mg_{2.6}Fe_{2.2}Al_{1.2}\ Si_{2.8}Al_{1.2}O_{10}(OH)_8$	5
(17) Collinsite $Ca_2(Mg, Fe)/(PO4)_2\ 2H_2O$	9
(18) Akaganite β-FeOOH	3
(19) Lepidocrocite FeO(OH)	3
(20) Gibbsite $Al(OH)_3$	6

Table 3B (Continued):

	Phases	Number of times appeared
(21)	Pyrolusite MnO	3
(22)	Siderite $FeO.CO_2$	1
(23)	Calcium Aluminum Silicate $Ca\ Al_2SiO_6$	6

TABLE 3C

SAMPLE - SPIRAL CONCENTRATE

21.3	10	4.180	γ-Fe_2O_3 Maghemite (C) 4.18 (200) Grunerite 4.16 (220) Tremolite 4.20 (220) Goethite 4.18 (110)
24.2	20	3.6746	Hematite 3.66 (012) Kirschsteinite 3.672 (111)
26.6	100	3.34	Vivianite 3.33 ($\bar{2}21$) Quartz 3.342 (101) Alunite 3.34 ($FeSiO_3$(M) 3.35 (021) $FeSiO_3$ (OR) 3.34 (121) Kyanite 3.35 (200)
33.3	100	2.696	Hematite 2.69 (104) Goethite 2.69 (130) Kyanite 2.694 ($21\bar{1}$) Tremolite 2.705 (151) Vivianite 2.71 (041) Kirschsteinite 2.687 (131) Chlorite 2.8 ($20\bar{1}$) Collinsite 2.69 ($\bar{1}21$, $1\bar{2}1$)
35.4	50	2.531	Magnetite 2.532 (311) Collinsite 2.54 (012) Maghenite (T) 2.521 (119,3$\bar{1}$3) Maghemite (C) 2.52 (311) Verculate 2.525 (202, $20\bar{4}$) Akaganite 2.543 (211) Vivianite 2.52 ($\bar{2}41$) Kyanite 2.52 (012, $11\bar{2}$)

Table 3C (Continued):

			Tremolite 2.529 ($\bar{2}02$, 002) Goethite 2.52 (101)
35.7	80	2.51	Calcium Aluminum Silicate 2.509 (131) Hematite 2.51 (110) Goethite 2.49 (040) Fe-Silicate (OR) 2.51 (202,430) Grunerite 2.507 ($20\bar{2}$) Kyanite 2.509 (030)
49.5	30	1.8394	Hematite 1.838 (024) Grunerite 1.837 (191, 0100) Lepidocrocite 1.848 (220) Kirschsteinite 1.835 (240,222) Maghemite (T) 1.835 (442) Collinsite 1.831 (831)
54.3	45	1.69	Hematite 1.69 (116) Goethite 1.694 (240) Tremolite 1.686 (003,281) Gibbsite 1.689 (314) Grunerite 1.685 ($51\bar{2}$) Vermiculite 1.695 (314) Maghemite (T) 1.702 (426) Collinsite 1.695 ($20\bar{3}$)

TABLE 3D

SAMPLE SPIRAL CONCENTRATE

Name of the Compound	Number of times appeared
Magnetite	2
Hematite	5
Maghemite (C)	2
Maghemite (T)	3
Goethite	5
Quartz	2
Gruneinite	4
Tremolite	4
Kirschsteinite	3
Vermiculate	2
Vivianite	3
Alunite	1
Fe-Silicate (M)	1
Fe-Silicate (OR)	2
Kyanite	4
Chlorite	1
Collinsite	4
Akaganite	1
Lepidocrocite	1
Gibbsite	1
Pyrolusite	0
Siderite	0
Calcium Aluminum Silicate	1

TABLE 3E

SAMPLE-SMS TAIL

Angle	Relative Intensity	dA°	Possible Mineral Phases
19.2	10	4.6187	Calcium Aluminum Silicate 4.62 (200) Fe-Silicate (OR) 4.62 (020) Fe-Silicate (M) 4.61 (020) Chlorite 4.62 (02.11)
19.9	10	4.4577	Vermiculate 4.41 ($\bar{1}12$) Kyanite 4.42 (110)
20.3	10	4.3708	Gibbsite 4.35 (110) Vermiculate 4.35 (022, 112)
20.8	20	4.2669	Quartz 4.26 (100) Vermiculate 4.25 (022 or 112)
21.3	30	4.18	Maghemite (C) 4.18 (200) Tremolite 4.20 (220) Goethite 4.18 (110)
21.4	30	4.1678	Grunerite 4.16 (220)
24.2	12	3.6746	Hematite 3.66 (012) Kirschsteinite 3.672 (111)
26.6	50	3.34	Vivanite 3.33 ($\bar{2}21$) Quartz 3.343 (101) Alunite 3.34 ($FeSiO_3$ (M) 3.35 (021) $FeSiO_3$ (OR) 3.34 (121) Kyanite 3.35 (200)
30.25	100	2.9520	Calcium Aluminum Silicate 2.94 ($\bar{2}21$) Magnetite 2.967 (220) Maghemite (T) 2.95 (206, 220)

Table 3E (Continued):

Angle	Relative Intensity	dA°	Possible Mineral Phases
			Kirschsteinite 2.957 (130)
			Kyanite 2.947 (120, 2$\bar{2}$0)
33.3	70	2.696	Hematite 2.69 (104)
			Goethite 2.69 (130)
			Kyanite 2.694 (21$\bar{1}$)
			Tremolite 2.705 (151)
			Vivianite 2.71 (041)
			Kirschsteinite 2.687 (131)
			Chlorite 2.68 (20$\bar{1}$)
			Collinsite 2.69 ($\bar{1}$21, 1$\bar{2}$1)
34.1	20	2.6262	Grunerite 2.639 (061)
			Akaganite 2.616 (400)
			Kirschsteinite 2.612 (112)
			Vermiculite 2.615 (13$\bar{2}$, 200)
			Chlorite 2.61 (20$\bar{2}$)
			Maghemite (C) 2.64 (310)
35.4	50	2.53	Magnetite 2.532 (311)
			Collinsite 2.54 (012)
			Maghemite (T) 2.521 (119,313)
			Maghemite (C) 2.52 (311)
			Vermiculite 2.525 (202, 20$\bar{4}$)
			Akaganite 2.543 (211)
			Vivianite 2.52 ($\bar{2}$41)
			Kyanite 2.52 (012, 11$\bar{2}$)
			Tremolite 2.529 ($\bar{2}$02, 002)
			Goethite 2.52 (101)

Table 3E (Continued):

Angle	Relative Intensity	dA°	Possible Mineral Phases
35.7	45	2.51	Hematite 2.51 (110) Goethite 2.49 (040) Fe-Silicate (OR) 2.51 (202, 430) Grunerite 2.507 ($20\bar{2}$) Kyanite 2.509 (030) Calcium Aluminum Silicate 2.509 ($\bar{1}31$)
36.7	45	2.453	Maghemite (T) 2.451 (305,314) Lepidocrocite (OR) 2.467 (031) Quartz 2.458 (110) **Gibbsite** 2.454 (021) Goethite 2.452 (111)
44.5	30	2.0337	$FeSiO_3$ (M) 2.039 (041) Grunerite 2.045 (351) Vermiculite 2.04 (208, 0014) Chlorite 2.045 (007) Maghemite (T) 2.026 (403,410) Tremolite 2.015 (202) Gibbsite 2.043 ($31\bar{3}$)
49.7	30	1.8325	Hematite 1.838 (024) Grunerite 1.837 (191, 0100) 5 Lepidocrocite 1.848 (220) Kirschsteinite 1.835 (240,222) Maghemite (T) 1.835 (442) Collinsite 1.831 (031)
53.3	10	1.7143	Goethite 1.721 (221) Grunerite 1.724 (082) Akaganite 1.719 (501, 431) Magnetite 1.7146 (422)

Table 3E (Continued):

Angle	Relative Intensity	dA°	Possible Mineral Phases
54.3	30	1.69	Hematite 1.69 (116) Goethite 1.694 (240) Tremolite 1.686 (003, 282) Gibbsite 1.689 (314) Grunerite 1.685 ($51\bar{2}$) Vermiculate 1.695 (314) Maghemite (T) 1.702 (42$\bar{0}$) Collinsite 1.695 (203)

TABLE 3F

SAMPLE SMS TAIL

Compound Name	No. of Times	Compound Name	No. of Times
Magnetite	3	Vermiculate	7
Hematite	5	Vivianite	3
Maghemite (C)	4	Alumite	1
Maghemite (T)	7	Fe-Silicate (M)	3
Goethite	5	Fe_2SiO_3 (OR)	3
Quartz	3	Kyanite	5
Grunerite	7	Chlorite	4
Tremolite	5	Collinsite	4
Kirschsteinite	5	Akaganite	3
Gibbsite	4	Pyrohisite	0
Siderite	0	Calcium Aluminum Silicate	3

TABLE 3G

SAMPLE-SPIRAL TAIL

Angle	Relative Intensity	dA°	Possible Mineral Phases
21°0	8	4.22	Tremolite 4.20 Kirschsteinite 4.22
21°3	8	4.167	γ -Fe_2O_3 Maghemite (C) 4.18 (200) Grunerite 4.16 (220) Goethite 4.18 (110)
24.1 to 24.5	6	3.70 to 3.63	Hematite 3.66 (012) Kirschsteinite 3.672 (111) Akaganite 3.70 (220) Vivianite 3.65 (111) Calcium Aluminum Silicate 3.63(111)
26.6	100	3.34	Vivianite 3.33 (221) Quartz 3.345 (101) Alunite 3.34 $FeSiO_3$ (M) 3.35 (021) $FeSiO_3$ (OR) 3.34 (121) Kyanite 3.35 (200)
33.3	12	2.696	Hematite 2.69 (104) Goethite 2.69 (130) Kyanite 2.694 ($21\bar{1}$) Tremolite 2.705 (151) Vivianite 2.71 (041) Kirschsteinite 2.687 (131) Chlorite 2.68 ($20\bar{1}$) Collinsite 2.69 ($\bar{1}21$,$1\bar{2}1$)

TABLE 3G

SAMPLE-SPIRAL TAIL

Angle	Relative Intensity	dA°	Possible Mineral Phases
21°0	8	4.22	Tremolite 4.20 Kirschsteinite 4.22
21°3	8	4.167	γ -Fe_2O_3 Maghemite (C) 4.18 (200) Grunerite 4.16 (220) Goethite 4.18 (110)
24.1 to 24.5	6	3.70 to 3.63	Hematite 3.66 (012) Kirschsteinite 3.672 (111) Akaganite 3.70 (220) Vivianite 3.65 (111) Calcium Aluminum Silicate 3.63(111)
26.6	100	3.34	Vivianite 3.33 (221) Quartz 3.345 (101) Alunite 3.34 $FeSiO_3$ (M) 3.35 (021) $FeSiO_3$ (OR) 3.34 (121) Kyanite 3.35 (200)
33.3	12	2.696	Hematite 2.69 (104) Goethite 2.69 (130) Kyanite 2.694 ($21\bar{1}$) Tremolite 2.705 (151) Vivianite 2.71 (041) Kirschsteinite 2.687 (131) Chlorite 2.68 ($20\bar{1}$) Collinsite 2.69 ($\bar{1}21$,$1\bar{2}1$)

Table 3G (Continued):

Angle	Relative Intensity	dA°	Possible Mineral Phases
35.7	8	2.51	Calcium Aluminum Silicate 2.509 (131) Hematite 2.51 (110) Goethite 2.49 (040) Fe-Silicate (OR) 2.51 (202,430) Grunerite 2.507 ($20\bar{2}$) Kyanite 2.509 (030)
36.7	10	2.458	Maghemite (T) 2.451 (305,314) Lepiodocrocite 2.467 (031) Quartz 2.458 (110) Gibbsite 2.454 (021) Goethite 2.452 (111)
39.6	6	2.2733	Kyanite 2.275 ($02\bar{2}$, $1\bar{2}2$) Hematite 2.285 (006) Calcium Aluminum silicate 2.27 (311) Tremolite 2.273 (112) Gibbsite 2.285 ($31\bar{2}$) Quartz 2.282 (102) Akaganite 2.285 (301) Vermiculate 2.265 (220,136) Chlorite 2.27 ($20\bar{4}$) Collinsite 2.25
40.4	4	2.23	Maghemite (T) 2.234 (316,219) Maghemite (C) 2.23 (321) Vivianite 2.23 Quartz 2.237 (111) Gruneirite 2.225 ($31\bar{2}$) Gibbsite 2.244 (022, 213) Kyanite 2.23 (300)

Table 3G (Continued):

Angle	Relative Intensity	dA°	Possible Mineral Phases
41.3	2	2.1836	Kirschsteinite 2.176 (132) Vermiculate 2.170 (206, Kyanite 2.181 ($22\bar{1}$, $3\bar{2}1$) Goethite 2.192 (140) Tremolite 2.181 ($44\bar{1}$) Vivianite 2.19
42.6	6	2.1199	Fe-Silicate (OR) 2.134 (630,502) Quartz 2.128 (200) Pyrolusite 2.13 (111) Siderite 2.13 (113) Collinsite 2.13 (030,$0\bar{3}1$) Magnetite 2.00 (400)
47.8	4	1.9008	Vivianite 1.89 Grunerite 1.912 ($42\bar{2}$) Chlorite 1.91 ($20\bar{6}$) Collinsite 1.91
50.3	10	1.817	Maghemite 1.822 (T) (416,423) Pyrolusite 1.81 Vivianite 1.82 Quartz 1.817 (112) Tremolite 1.814 (530)
54.3	6	1.69	Hematite 1.69 (116) Goethite 1.694 (240) Tremolite 1.686 (003,282) Gibbsite 1.689 (314) Grunerite 1.685 ($51\bar{2}$) Vermiculate 1.695 (314) Maghemite (T) 1.702 (426) Collinsite 1.695 ($20\bar{3}$)

Table 3G (Continued):

Angle	Relative Intensity	dA°	Possible Mineral Phases
55.1	5	1.6678	Calcium Aluminum Silicate 1.662 ($\bar{3}13$) Maghemite (T) 1.669 (500,409) Chlorite 1.67 (206) Vermiculate 1.665 (2014) Goethnite 1.661 (060) Quartz 1.672 (202) Vivianite 1.67 Collinsite 1.669 ($\bar{1}13$,$\bar{1}40$)
60.05	8	1.5402	Calcium Aluminum Silicate 1.540 (600) Vermiculate 1.543 (20,14) Quartz 1.541 (211)
60.1	8	1.5379	Lepidocrocite 1.535 (802) Maghemite (C) 1.53 (521)
64.2	6	1.4492	Pyrite 1.4448 (321) Lepidocrocite 1.449 (180)
68.3	9	1.3709	Siderite 1.373 (125) Akaganite 1.374 (730, 312) Quartz 1.372 (301)

TABLE 3H

SAMPLE-SPIRAL TAIL

Name of the Compound	Number of times appeared
Magnetite	0
Hematite	5
Maghemite (C)	1
Maghemite (T)	5
Goethite	7
Quartz	8
Grunerite	4
Tremolite	5
Kirschsteinite	4
Vermiculate	5
Vivianite	6
Alunite	0
Fe-Silicate (M)	1
Fe-Silicate (OR)	2
Kyanite	6
Chlorite	4
Collinsite	6
Akaganite	3
Lepidocrocite	3
Gibbsite	4
Pyrolusite	2
Siderite	1
Calcium Aluminum Silicate	5
Pyrite	1

TABLE 3I

SAMPLE-SPIRAL TAIL SUBJECTED TO MAGNETIC SEPARATION

MAGNETIC FRACTION

Angle	Relative Intensity	dA°	Possible Mineral Phases
21.3	45	4.18	γ-Fe_2O_3 Maghemite (C) 4.18 (200) Grunerite 4.167 (220) Tremolite 4.20 (220) Goethite 4.18 (110)
26.6	50	3.34	Vivianite 3.33 ($\bar{2}21$) Quartz 3.343 (101) Alunite 3.34 ($FeSiO_3$(M) 3.35 (021) $FeSiO_3$ (OR) 3.34 (121) Kyanite 3.35 (200)
30.0	25	2.975	Vivianite 2.97 (201) Magnetite 2.867 (220)
30.2	40	2.95	Calcium Aluminum Silicate 2.94 ($\bar{2}21$) Maghemite (T) 2.95 (206, 220) Kirschsteinite 2.957 (130) Kyanite 2.947 (120, $2\bar{2}0$)
33.3	80	2.696	Hematite 2.69 (104) Goethite 2.69 (130) Kyanite 2.694 ($21\bar{1}$) Tremonite 2.705 (151) Vivianite 2.71 (041) Kirschsteinite 2.687 (131) Chlorite 2.68 ($20\bar{4}$) Collinsite 2.69 ($\bar{1}21$, $1\bar{2}1$)

Table 3I (Continued):

Angle	Relative Intensity	dA°	Possible Mineral Phases
35.4	100	2.53	Magnetite 2.532 (311) Maghemite (T) 2.521 (119,313) Maghemite (C) 2.52 (311) Akaganite 2.543 (211) Vivianite 2.52 ($\bar{2}41$) Collinsite 2.54 (012) Vermiculate 2.525 (204, $20\bar{4}$) Kyanite 2.52 (012, $11\bar{2}$) Tremolite 2.529 ($\bar{2}02$,002) Goethite 2.52 (101)
35.7	70	2.51	Hematite 2.51 (110) Goethite 2.49 (040) Fe-Silicate (OR) 2.51(202,430) Grunerite 2.507 ($20\bar{2}$) Kyanite 2.509 (030) Calcium Aluminum Silicate 2.509 ($\bar{1}31$)
36.7	30	2.453	Maghemite (T) 2.451 (305,314) Lepidocrocite 2.467 (031) Quartz 2.458 (110) Gibbsite 2.454 (021) Goethite 2.452 (111)
43.2	20	2.09	Magnetite 2.0993 (400) Maghemite (T) 2.089 (400) Maghemite (C) 2.08(400) Chlorite 2.10 ($20\bar{5}$) Vermiculate 2.08 (138) Lepidocrocite 2.09 (130,060) Akaganite 2.09 (321)

Table 3I (Continued):

Angle	Relative Intensity	dA°	Possible Mineral Phases
			Gibbsite 2.085 (114)
			Collinsite 2.10 ($1\bar{1}2$, $12\bar{2}$)
53.3	15	1.7143	Goethite 1.721 (221)
			Grunerite 1.724 (082)
			Akaganite 1.719 (501,431)
			Magnetite 1.7146 (422)
			Maghemite (T) 1.702 (426)
			Maghemite (C) 1.70 (422)
54.3	12	1.69	Hematite 1.69 (116)
			Goethite 1.694 (240)
			Tremolite 1.686 (003, 282)
			Gibbsite 1.689 (314)
			Grunerite 1.685 ($51\bar{2}$)
			Vermiculate 1.695 (314)
			Maghemite (T) 1.702 (426)
			Collinsite 1.695 (203)
57.0	35	1.6148	Magnetite 1.6158 (511)
			Maghemite (C) 1.61 (511,333)
			Kirschsteinite 1.610 (062,004)
62.6	50	1.484	Magnetite 1.484 (440)
			Maghemite (C) 1.481 (440)
			Hematite 1.484 (300)
64.2	12	1.4495	Pyrite 1.4448 (321)
			Lepidocrocite 1.449 (180)

TABLE 3J

SAMPLE-MAGNETIC PORTION OF SPIRAL TAIL

	Conc. (Mag.)
Magnetite	6
Hematite	4
Maghemite (C)	6
Maghemite (Tetragonal)	6
Goethite	6
Quartz	2
Grunerite	4
Tremolite	3
Kirschsternite	3
Vermiculate	3
Vivianite	4
Alunite	1
Fe-Silicate (M)	1
Fe-Silicate (OR)	2
Kyanite	5
Chlorite	2
Collinsite	4
Akaganite	3
Lepidocrocite	3
Gibbsite	3
Prysohisite	0
Pyrohotite	0
Calcium Aluminum Silicate	2
Pyrite	1

TABLE 3K

NONMAGNETIC PORTION OF SPIRAL TAIL

Angle	Relative Intensity	dA°	Possible Mineral Phases
16.5	12	5.3679	Maghemite (T) 5.37 (112)
20.9	16	4.26	Quartz (4.26) (100) Vermiculite 4.25 (022 or 112)
21.3	12	4.18	-Maghemite (C) 4.18 (200) Grunerite (4.16) (220) Tremolite 4.20 (220) Goethite 4.18 (110)
24.0-24.2	12	3.70-3.66	Akaganite 3.70 (220) Hematite 3.66 (012) Kirschsteinite 3.672 (111)
26.6	100	3.34	Quartz 3.343 (101) Alunite 3.34 $FeSiO_3$(M) 3.35 (021) $FeSiO_3$ (OR) 3.34 (121) Kyanite 3.35 (200) Vivianite 3.33 ($\bar{2}21$)
33.3	25	2.69	Hematite 2.69 (104) Goethite 2.69 (130) Kyanite 2.894 (21$\bar{1}$) Tremolite 2.705 (151) Vivianite 2.71 (041) Kirschsteinite 2.687 (131) Chlorite 2.682 (20$\bar{1}$) Collinsite 2.69 ($\bar{1}21$, $1\bar{2}1$)

Table 3K (Continued):

Angle	Relative Intensity	dA°	Possible Mineral Phases
35.4	6	2.53	Magnetite 2.532 (311) Maghemite (T) 2.521 (012) Maghemite (C) 2.52 (119,313) Vermiculate 2.525 (311) Akaganite (2.543) (202, 20$\bar{4}$) Vivianite 2.52 (211) Collinsite 2.54 ($\bar{2}$41) Kyanite 2.52 (012, 11$\bar{2}$) Tremolite 2.529 ($\bar{2}$02, 002) Goethite 2.52 (101) Calcium Aluminum Silicate 2.535 ($\bar{2}$.02, 002)
35.7	16	2.51	Calcium Aluminum Silicate 2.509($\bar{1}$31) Hematite 2.51 (110) Goethite 2.49 (040) Fe-Silicate (OR) 2.51(202,430) Grunerite 2.507 (20$\bar{2}$) Kyanite 2.509 (030)
36.7	37	2.458	Maghemite (T) 2.509 ($\bar{1}$31) Lepidocrocite (OR) 2.49 (110) Quartz 2.51 (040) Gibbsite 2.507 (202,430) Kyanite 2.509 (030).
39.56	16	2.2733	Kyanite 2.272 (02$\bar{2}$, 1$\bar{2}\bar{2}$) Hematite 2.285 (006) Calcium Aluminum Silicate 2.27(31[illegible] Tremolite 2.273 (112) Gibbsite 2.285 (31$\bar{2}$) Quartz 2.282 (102)

Table 3K (Continued):

Angle	Relative Intensity	dA°	Possible Mineral Phases
			Akaganite 2.285 (301) Vermiculate 2.265(220,136) Chlorite 2.27 ($20\bar{4}$) Collinsite 2.25
40.4	10	2.23	Maghemite (T) 2.234 (316,219) Maghemite (C) 2.23 (321) Vivianite 2.23 Quartz 2.237 (111) Grunerite 2.225 (312) Gibbsite 2.244 (022,213) Kyanite 2.23 (300)
42.5	8	2.12	Fe-Silicate (OR) 2.134 (130,502) Quartz 2.128 (200) Pyrolusite 2.13 (111) Siderite 2.13 (113) Collinsite 2.13 (030,$0\bar{3}1$)
45.9	6	1.98	Pyrolusite 1.98 (210) Fe-Silicate (OR) 1.995 (440,241) Maghemite (T) 1.994 (412) Gibbsite 1.993 (023) Grunerite 1.996 (190, 370) Quartz 1.98 (201) Vermiculate 1.975 (13 10)
50.3	36	1.817	Quartz 1.817 (112) Maghemite (T) 1.822 (416, 423) Viviauite 1.82 Pyrolusite 1.81 Tremolite 1.814 (530)

Table 3K (Continued):

Angle	Relative Intensity	dA°	Possible Mineral Phases
53.3	34	1.7143	Goetnite 1.721 (221) Grunerite 1.724 (082) Akaganite 1.719 (501,431) Magnetite 1.7146 (422) Maghemite (T) 1.702 (426) Maghemite (C) 1.70 (422)
54.3	4	1.69	Hematite 1.69 (116) Goethite 1.694 (240) Tremolite 1.68 (003, 282) Gibbsite 1.68 (314) Grunerite 1.685 (51$\bar{2}$) Vermiculite 1.695 (314) Maghemite (T) 1.702 (426) Collinsite 1.695 (203)
60.0-60.1	30	1.5402-1.5379	Calcium Aluminum Silicate 1.540(600) Vermiculite 1.543 (210 14) Quartz 1.541 (211) Lepidocrocite 1.535 (802) Maghemite (C) 1.53 (521)
64.05	10	1.452	Pyrite 1.4498 (321) Lepidocrocite 1.449 (180)
67.7	12	1.3802	Quartz 1.382 (212)
68.15	22	1.375	Quartz 1.375 (203)
68.35	18	1.372	Quartz 1.372 (301)

TABLE 3L

SAMPLE-NONMAGNETIC PORTION OF SPIRAL TAIL

	Tailing (Nonmagnetic)
Magnetite	2
Hematite	5
Maghemite (C)	5
Maghemite (Tetragonal)	8
Goethite	6
Quartz	10
Grunerite	6
Tremolite	6
Kirschsternite	2
Vermiculate	5
Vivianite	5
Alunite	1
Fe-Silicate (M)	1
Fe-Silicate (OR)	3
Kyanite	6
Chlorite	2
Collinsite	5
Akaganite	4
Lepidocrocite	3
Gibbsite	5
Pyrrhotite	3
Siderite	0
Calcium Aluminum Silicate	4
Pyrite	0

TABLE 3M

SAMPLE- RED PARTICLES PICKED FROM SPIRAL TAIL

2θ in degrees	Relative Intensity	d values	Compounds with the corresponding d values
20.8	25	4.267	Quartz 4.26 (100) Vermiculate 4.25 (022 or 112)
21.3	30	4.18	Maghemite (C) 4.18 (200) Grunerite 4.16 (220) Tremolite 4.20 (220) Goethite 4.18 (110)
24.2	35	3.67	Hematite 3.66 (012) Kirschsteinite 3.67 (111)
25.1	20	3.5587	Vermiculate 3.56 (008) Chlorite 3.55 (004)
26.6	20	3.34	Vivianite 3.33 ($\bar{2}21$) Quartz 3.343 (101) Alunite 3.34 ($FeSiO_3$ (M) 3.35 (021) $FeSiO_3$ (OR) 3.34 (121) Kyanite 3.35 (200)
31.2	50	2.8633	Maghemite (T) 2.87 (222) Chlorite 2.87 (005) Vermiculate 2.85 (0010) Calcium Aluminum Silicate 2.86 (311)
33.3	100	2.696	Hematite 2.69 (104) Goethite 2.69 (130) Kyanite 2.694 ($21\bar{1}$) Tremolite 2.705 (151) Vivianite 2.71 (041)

Table 3M (Continued):

2θ in degrees	Relative Intensity	d values	Compounds with the corresponding d values
			Kirschsteinite 2.687 (131)
			Chlorite 2.68 ($20\bar{1}$)
			Collinsite 2.69 ($\bar{1}21$, $1\bar{2}1$)
33.6	40	2.664	Chlorite (200)
35.4	50	2.53	Magnetite 2.532 (311)
			Collinsite 2.54 (012)
			Maghemite (T) 2.521 (119,313)
			Maghemite (C) 2.52 (311)
			Vermiculate 2.525 (202,205)
			Akaganite 2.543 (211)
			Vivianite 2.52 ($\bar{2}41$)
			Calcium Aluminum Silicate 2.535 ($\bar{2}02$,002)
			Kyanite 2.8 (012, $11\bar{2}$)
			Tremolite 2.529 ($\bar{2}02$, 002)
			Goethite 2.52 (101)
35.7	30	2.51	Calcium Aluminum Silicate 2.509 ($\bar{1}31$)
			Hematite 2.51 (110)
			Goethite 2.49 (040)
			Fe-Silicate (OR) 2.51 (202,430)
			Grunerite 2.507 ($20\bar{2}$)
			Kyanite 2.509 (030)
37.0	25	2.4208	Magnetite 2.4243 (222)
40.9	25	2.2040	Vivianite 2.19
			Grunerite 2.20 (261, $24\bar{2}$)
			Tremolite 2.206 ($\bar{2}42$, 042)
			Goethite 2.19 (140)
			Hematite 2.201 (006)

Table 3M (Continued):

2θ in degrees	Relative Intensity	d values	Compounds with the corresponding d values
49.5	40	1.8394	Hematite 1.838 (024) Grunerite 1.837 (191,0100) Lepidocrocite 1.848 (220) Kirschiteinite 1.835 (240,222) Maghemite (T) 1.835 (442) Collinsite 1.831 (031)
54.3	50	1.69	Hematite 1.69 (116) Goethite 1.694 (240) Tremolite 1.686 (003,282) Gibbsite 1.69 (314) Grunerite 1.685 ($51\bar{2}$) Vermiculite 1.695 (314) Maghemite (T) 1.702 (426) Collinsite 1.695 ($20\bar{3}$)
64.1	45	1.45	Pyrite 1.4448 (321) Lepidocrocite 1.449 (180)

TABLE 3N

SAMPLE RED PARTICLE PICKED FROM SPIRAL TAIL

Compounds	Red Particle
Magnetite	2
Hematite	6
Maghemite (C)	2
Maghemite (T)	4
Goethite	6
Quartz	2
Grunerite	5
Tremolite	4
Kirschsteinite	3
Vermiculate	3
Vivianite	3
Alunite	1
Fe-Silicate (M)	1
Fe-Silicate (OR)	2
Kyanite	2
Chlorite	3
Collinsite	4
Akaganite	1
Lepidocrocite	2
Gibbsite	1
Pyrolusite	0
Siderite	0
Calcium Aluminum Silicate	3
Pyrite	1

TABLE 30'

SAMPLE BLACK PARTICIE PICKED FROM SPIRAL TAIL

2θ	Relative Intensity	d value A°	Compounds
13.6	20	6.5053	Fe-silicate (OR) (210)
21.3	40	4.18	Maghemite (C) 4.18 (200) Grunerite 4.16 (220) Tremolite 4.20 (220) Goethite 4.18 (110)
24.2	20	3.67	Hematite 3.66 (012) Kirschsteinite 3.672 (111)
26.6	15	3.34	Quartz 3.343 (101) Vivianite 3.33 ($\bar{2}21$) Alunite 3.34 (Fe-Silicate (M) 3.35 (021) Fe-Silicate (OR) 3.34 (121) Kyanite 3.35 (200)
27.6	15	3.2291	Fe-Silicate (M) 323 (220) Maghemite (T) 3.216 (214,205)
28.4	15	3.1399	Colliusite 3.14 (101) Pyrite 3.128 (111) Pyrolusite 3.14 (110)
29.1	10	3.07	Grunerite 3.07 (060, 310) Maghemite (T) 3.07 (117)
29.4	10	3.035	Colliusite 3.04 ($0\bar{2}1$) Fe-Silicate (M) 3.03 ($22\bar{1}$) Tremolite 3.03 ($31\bar{1}$, $24\bar{1}$)

Table 3'0' (Continued):

2θ	Relative Intensity	d value A°	Compounds
30.4	20	2.9368	Calcium Aluminum Silicate 2.94 ($\bar{2}21$) Kyanite 2.947 (120, $2\bar{2}0$) Tremolite 2.938 ($\bar{1}51$) Maghemite (C) 2.95 (220) Maghemite (T) 2.95 (206,220)
31.3	20	2.8633	Maghemite (T) 2.87 (222) Chlorite 2.87 (005) Vermiculite 2.85 (0010) Calcium Aluminum Silicate 2.863(311)
31.6	20	2.828	Chlorite 2.84 (005)
33.3	100	2.69	Hematite 2.69 (104) Goethite 2.69 (130) Kyanite 2.694 ($21\bar{1}$) Tremotite 2.705 (151) Vivianite 2.71 (041) Kirschsteinite 2.687 (131) Chlorite 2.68 ($20\bar{1}$) Collinsite 2.69 ($\bar{1}21$, $1\bar{2}1$)
35.4	60	2.53	Magnetite 2.532 (311) Collinsite 2.54 (012) Maghemite (T) 2.521 (119, 313) Maghemite (C) 2.52 (311) Vermiculite 2.525 (202, $20\bar{4}$) Akaganite 2.543 (211) Vivianite 2.52 ($\bar{2}41$) Calcium Aluminum Silicate 2.535 (202, 002) Kyanite 2.52 (012, $11\bar{2}$) Tremolite 2.529 ($\bar{2}02$, 002)

Table 3'0' (Continued):

2θ	Relative Intensity	d value A°	Compounds
35.7	40	2.51	Calcium Aluminum Silicate 2.509($\bar{1}$31) Hematite 2.51 (110) Goethite 2.49 (040) Fe-Silicate (OR) 2.51(202,430) Grunerite 2.507 (20$\bar{2}$) Kyanite 2.509 (030)
36.7	25	2.45	Maghemite (T) 2.451 (305,314) Lepidocrocite 2.467 (031) Quartz 2.458 (110) Gibbsite 2.454 (021) Goethite 2.452 (111)
40.8	25	2.2040	Maghemite (T) 2.208 (307) Chlorite 2.20 (203) Pyrite 2.21 (211) Vermiculate 2.200 (206, 20$\bar{8}$+) Pyrolusite 2.21 (200) Vivianite 2.19 (Grunerite 2.20 (261, 24$\bar{2}$) Tremolite 2.206 ($\bar{2}$42, 042) Goethite 2.192 (140) Hemalite 2.20 (113) Calcium Aluminum Silicate 2.21 (112, $\bar{3}$12)
49.6	25	1.838	Hematite 1.838 (024) Grunerite 1.837 (191, 0100) Lepidocrocite 1.848 (220) Kirschsteinite 1.835 (240,222) Maghemite (T) 1.835 (442) Collinsite 1.831 (031)

Table 3'0' (Continued):

2θ	Relative Intensity	d value A°	Compounds
53.3	20	1.7143	Goethite 1.721 (221) Grunerite 1.724 (082) Akaganite 1.719 (501, 431) Magnetite 1.7146 (422) Maghemite (T) 1.702 (426) Maghemite (C) 1.70 (422)
54.3	18	1.69	Hematite 1.69 (116) Goethite 1.694 (240) Tremolite 1.686 (003, 282) Gibbsite 1.689 (314) Grunerite 1.685 (51$\bar{2}$) Vermiculate 1.695 (314) Maghemite (T) 1.702 (426) Collinsite 1.695 (203)
625	30	1.4845	Hematite 1.482 (300) Maghemite (C) 1.4310 (440) Maghetite 1.4845 (440)
64.0–64.2	40	1.4533–1.4492	Hematite 1.452 (300) Goethite 1.453 (061) Quartz 1.453 (113) Pyrite 1.4448 (321) Lepiodocrocite 1.449 (180)

TABLE 3P

SAMPLE- BLACK PARTICLE PICKED FROM SPIRAL TAIL

Compounds	Black Particle
Magnetite	3
Hematite	8
Maghemite (C)	4
Maghemite (T)	9
Goethite	9
Quartz	2
Grunerite	6
Tremolite	7
Kirschsteinite	2
Vermiculate	4
Vivianite	4
Alunite	1
Fe-Silicate (M)	3
Fe-Silicate (OR)	3
Kyanite	4
Chlorite	5
Collinsite	3
Akaganite	2
Lepidocrocite	3
Gibbsite	2
Pyrolusite	2
Siderite	0
Calcium Aluminum Silicate	5
Pyrite	3

TABLE 3Q

SAMPLE WHITE PARTICLE PICKED FROM SPIRAL TAIL

2θ	Relative Intensity	d value A°	Compounds
20.8	30	4.2669	Quartz 4.266 (100) Vermiculate 4.25 (022,112)
24.0	11	3.7049	
26.6	100	3.34	Quartz 3.34 (101) Alunite 3.34 (Kyanite 3.35 (200)
36.7	12	2.45	Quartz 2.458 (110)
39.6	12	2.2733	Quartz 2.282 (102)
40.4	6	2.235	Quartz 2.237 (111)
42.5	9	2.12	Quartz 2.128 (200)
45.9	6	1.98	Quartz 1.98 (201)
50.3	17	1.817	Quartz 1.817 (112)
55.1	7	1.665	Quartz 1.672 (202)
60.0	15	1.5402	Quartz 1.541 (211)
68.3	11	1.375	Quartz 1.372 (301)

This white particles contain almost quartz with trace of Alumite and Kyanite.

Abbreviations Used

M - Monoclinic

OR - Orthorhomtoic

C - Cubic

T - Tetragonal

APPENDIX D

TABLE 5A

PARTICLE SIZE DISTRIBUTION OF 0-20 μ MATERIAL OF SPIRAL TAIL

Size (μ)	wt%
25.	0.23
19.69	2.03
15.629	0.24
12.40	0.413
9.845	1.379
7.814	7.312
6.202	10.953
4.922	30.470
3.907	16.18
3.101	26.56
2.461	4.225

RESULTS OF MAGNETIC SEPARATION USING LABORATORY MAGNETIC SEPARATOR

Size	wt%	Mag.fraction in total	Nonmagnetic in total material	Mag:Nonmag. ratio	Solubility S_1	$W_1 S_1$	Recovery $\frac{(W_1 S_1)}{(\overline{W_1 S_1})^x}$
+35	21.630	0.79	20.840	1:26	84.3	18.23	34.79
-35+48	8.322	0.426	7.895	1:18.5	76.8	6.39	12.19
-48+65	12.100	0.478	11.622	1:24	51.0	6.17	11.77
-65+100	17.500	0.397	17.100	1:43	30.5	5.34	10.19
-100+200	28.890	0.776	28.110	1:36	29.6	8.55	16.31
-200+400	9.680	0.468	9.212	1:19.7	62.9	6.08	11.60
-400	1.865	0.177	1.688	1:9.5	88.2	1.64	3.12
	99.987	3.512	96.465	1:25		52.4	99.97

Acid solubility of magnetic fraction - 98.2%

Acid solubility of nonmagnetic fraction - 50.7%.

TABLE 5C

RESULTS OF MAGNETIC SEPARATION USING FRANTZ ISODYNAMIC SEPARATOR

Size/Fraction	Weight %	Solubility %	Recovery
+ 35 mesh	19.0	75.0	26.83
- 35 mesh Nonmagnetic	77.7	45.8	67.01
- 35 mesh magnetic	3.3	98.1	6.09
	100.0		99.93

TABLE 5D

RESULTS OF SETTLING EXPERIMENTS AT DIFFERENT DISPERSANT CONCENTRATION ON 0-7+ μ PARTICLE SYSTEM AT VARIOUS pH

P.D. 1%, Settling Time 5½ mins.

10 Mins. time for stabilising the pH 1 min conditioning time

pH	Conc. of Dispersant in ppm	wt.% Settled	Assay %	Recovery of valuable mineral in the conc.	Recovery of Gangue mineral in the tail	S_I
7.2	0	95.0	53.70	100.00	15.25	-
	20	93.6	54.00	100.00	17.04	-
	40	92.0	52.80	100.00	16.33	-
	80	87.7	53.76	98.00	3.70	-
9.2	0	91.7	51.70	98.54	14.66	3.400
	20	87.8	54.80	100.00	23.53	-
	40	86.8	50.70	91.47	17.54	1.510
	80	85.7	52.63	93.76	21.78	2.019
11.2	0	87.6	53.54	97.50	21.58	3.2
	20	84.2	51.90	90.83	21.96	1.649
	40	84.1	51.73	90.43	21.62	1.643
	80	82.2	53.20	90.91	25.87	1.868

Solubility of Startin Material 48.1

TABLE 5E

RESULTS OF SETTLING EXPERIMENTS WITH STARVATION DOSAGE STARCH AT DIFFERENT DISPERSANT CONCENTRATION ON 0-74μ PARTICLE SYSTEM

P.D. 1.25%, Conditioning time 10 min; Settling time 1 min.

Dispersion addition	Taping Port	Weight %	Assay % Fe_2O_3	Recovery		Cumulative Binary Cut Assay		Selectivity Index
				Soluble Fe_2O_3	Total Insoluble SiO_2	Fe_2O_3	SiO_2	
1000 ppm	T_1	7.74	54.90	7.69	7.02	5.42	49.69	-
+	T_2	16.83	56.25	17.04	19.04	55.47	50.08	0.9050
2 ppm	T_3	9.76	55.75	9.81	14.81	55.31	48.72	1.03
MCH Starch	T_4	65.65	55.25	65.44	59.11	55.25	44.75	1.149
100 ppm	T_1	8.92	59.50	8.40	9.81	63.01	40.41	-
+	T_2	15.54	56.10	13.83	15.36	62.86	38.54	1.08
2 ppm	T_3	7.41	57.80	6.78	8.49	64.88	34.94	1.176
MCH Starch	T_4	68.08	65.85	70.98	63.13	65.85	34.15	1.194
10 ppm	T_1	3.71	54.00	3.79	3.99	57.30	42.68	-
+	T_2	8.91	50.10	8.44	10.41	57.42	42.81	0.973
2 ppm	T_3	2.43	54.05	2.48	2.61	58.18	42.04	1.15
MCH Starch	T_4	84.94	58.30	93.72	82.92	58.30	41.70	1.75

MCH Starch: Modified Caustisized Homogenised Starch.

TABLE 5F

RESULTS OF II STAGE SETTLING EXPERIMENTS ON PARTICLE SYSTEM. 0-74μ USING CONSTANT DISPERSANT CONCENTRATION

Weight %	Assay Fe_2O_3,%	Recovery R_{vm}	Recovery R_{1vm}	Selectivity Index
46.00	72.00	62.49	72.59	2.100

TABLE 5G

RESULTS OF FLOCCULATION EXPERIMENTS USING MODIFIED CAUSTICIZED STARCH AT DIFFERENT pH on 0-74 μ AT CONSTANT DISPERSANT CONCENTRATION

40 ppm P.D. 1% conditioning time 3 min settling time 1 min.

pH	Dispersant conc.40 ppm flocculant conc.in ppm	wt % settled	Assay Fe_2O_3 %	Recovery of Vol. Min. in Concen. %	Recovery of Gangue in Tail %	Selectivity Index
	30	81.8	52.40	89.11	24.97	1.650
	18	86.2	52.90	94.80	21.77	2.252
7.2	12	87.0	52.80	95.50	19.87	2.294
	6	87.3	52.11	94.57	19.44	2.031
	2	88.7	52.45	96.72	18.73	2.606
	30	73.6	51.76	78.74	31.6	1.305
	18	76.9	53.30	82.75	30.80	1.455
9.2	12	76.2	52.30	82.85	29.96	1.437
	6	76.2	52.20	82.69	29.81	1.424
	2	76.4	53.40	84.81	31.40	1.598
	30	74.9	52.80	82.20	31.88	1.470
	18	77.0	53.60	85.80	31.15	1.653
11.2	12	75.5	53.80	84.44	32.79	1.627
	6	77.2	54.27	87.10	31.97	1.781
	2	74.6	52.40	81.26	31.58	2.071

TABLE 5H

RESULTS OF FLOCCULATION EXPERIMENTS WITH MODIFIED CAUSTICIZED HOMOGENISED STARCH AT DIFFERENT pH AT CONSTANT DISPERSANT CONCENTRATION ON 0-74μ PARTICLE SYSTEM

P.D. 1% Conditioning Time 3 min; Settling time 1 min.

pH	Flocculant Conc.	Wt % Settled	Assay Fe_2O_3,%	Recovery of Vol. Min.	Recovery of valuable min.	Selectivity Index
9.0	5	75.0	56.40	87.94	36.99	2.060
	10	73.8	55.00	80.64	36.01	1.530
	20	76.2	50.90	80.64	27.91	1.269
	40	73.3	52.60	80.14	33.05	1.411
	80	72.9	52.50	79.56	33.28	1.393
	160	74.0	52.60	80.91	31.98	1.411
10.0	5	71.8	56.84	84.84	40.29	1.943
	10	70.8	55.20	81.24	38.88	1.659
	20	73.8	56.95	87.35	38.78	2.091
	40	70.7	52.08	76.54	34.72	1.317
	80	73.4	54.10	82.53	35.05	1.596
	160	73.2	55.44	84.36	37.29	1.790
11.0	5	71.6	57.00	84.84	40.67	1.958
	10	72.8	54.90	83.07	36.73	1.685
	20	72.3	57.40	86.27	40.65	2.074
	40	74.4	55.52	85.86	36.23	1.868
	80	73.7	53.33	81.70	33.72	1.507
	160	71.7	54.70	38.29	81.51	1.623

Acid solubility of starting material 48.1%
Conditioning time: 3min, settling time: 1min.

TABLE 5I

RESULTS OF FLOCCULATION EXPERIMENTS WITH DIFFERENT FLOCCULLANTS AT DIFFERENT CONCENTRATION AT CONSTANT DISPERSANT CONCENTRATION 50 ppm ON PARTICLE SYSTEM 0.74μ at pH 11

P.D. 1% Conditioning time: 3 min; Settling time: 1 min.

		Wt. settled %	Assay %	Recovery of valuable mineral	Recovery of less valuable mineral	Selectivity Index
1. Washing Expt.: The tail material is washed at pH 11.2 water for 3 or 4 times		88%	50.86	90.95	18.36	1.500
Flocculant	Concentration					
Amylopectin	40	73.7	56.98	85.34	38.90	1.925
	30	81.8	59.16	98.35	35.63	5.740
	20	78.8	56.34	90.22	33.71	2.165
	10	81.9	57.02	94.91	32.17	2.973
	5					
Polyacrylamide	40	81.0	57.65	94.91	33.90	3.090
	30	87.3	55.78	98.96	25.61	5.720
	20	81.9	54.33	90.43	27.93	1.913
	10	87.3	55.55	98.55	25.23	4.788
	5					
Xanthate introduced Polacrylamide	80	75.5	57.21	87.79	37.75	2.088
	60	81.5	55.46	91.86	29.33	2.164
	40	73.1	57.18	84.95	39.68	1.926
	20	72.4	56.36	82.93	39.12	1.766

Solubility in acid of starting material: 48.1%.

TABLE 5J

RESULTS OF FLOCCULATION EXPERIMENTS WITH DIFFERENT FLOCCULANTS AT CONSTANT DISPERSION CONCENTRATION ON 0-20μ PARTICLE SYSTEM AT pH 6.9

P.D. 1% Conditioning time: 3 min, Settling time: 1 min.

Sl. No.	Conc.of Flocculant	Flocculant used	Wt.Settled %	Assay Fe_2O_3 %	Recovery of valuable Min. in conc.(R_{vm})	Recovery of less valuable Min in tail (R_{lvm})	Selectivity Index
1	0	Modified Causticized Starch	42.9	57.10	50.92	64.53	1.887
2	10		48.7	60.00	60.74	62.46	1.604
3	20		42.2	59.24	51.97	66.85	1.477
4	30		44.0	62.72	57.37	68.39	1.706
5	40		37.2	71.23	55.08	79.37	2.121
6	10	Amylopectin	42.0	63.33	55.29	70.32	1.711
7	20		36.1	61.21	45.93	73.01	1.515
8	30		43.6	61.46	55.71	67.62	1.620
9	40		43.5	60.00	54.26	66.47	1.533
10	10	Xanthate introduced polymer	36.0	65.00	48.64	75.72	1.718
11	20		47.1	78.13	76.50	80.15	3.625
12	30		46.1	59.65	57.16	64.15	1.545
13	40		45.1	60.00	56.25	65.24	1.553
14	10	Polyacrylamide of high Molr.wt.	43.7	60.18	54.66	66.47	1.545
15	20		43.3	63.27	56.95	69.35	1.730
16	30		44.5	60.89	56.33	66.46	1.598
17	40		42.3	62.64	55.08	69.55	1.673

Continued....

Table 5J (Continued):

Sl. No.	Conc.of Floccu-lant	Floccu-lant used	Wt.Settled %	Assay Fe_2O_3 %	Recovery of valuable Min. in conc.(R_{vm})	Recovery of less valuable Min.in tail (R_{lvm})	Selectivity Index
18	10	Polyacry-	44.3	62.30	57.37	67.82	1.684
19	20	lamide of	51.4	60.90	65.07	61.27	1.715
20	30	medium	47.7	60.16	59.69	63.38	1.600
21	40	Molr.wt.	46.5	61.07	59.03	65.12	1.640
22	10	Polyacry-	44.2	59.95	55.08	65.93	1.540
23	20	lamide of	47.5	60.21	59.37	63.39	1.590
24	30	low Molr.	46.5	61.23	59.19	65.26	1.650
25	40	wt.	45.5	58.46	55.30	63.58	1.469

TABLE 5K

RESULTS OF II STAGE FLOCCULATION EXPERIMENT AT CONSTANT DISPERSANT CONCENTRATION, AT CONSTANT FLOCUULANT CONCENTRATION (XANTHATE INTRODUCED POLYACRYLAMIDE) AT pH 6.9 WITH PARTICLE SYSTEM 0-20

P.D. 1% Conditioning time - 3 min, Settling time - 1 min,

Weight %	Assay Fe_2O_3 %	Recovery R_{vm}	Recovery of less valuable mineral	Selectivity Index
44.3	81.00	74.60	83.63	3.873

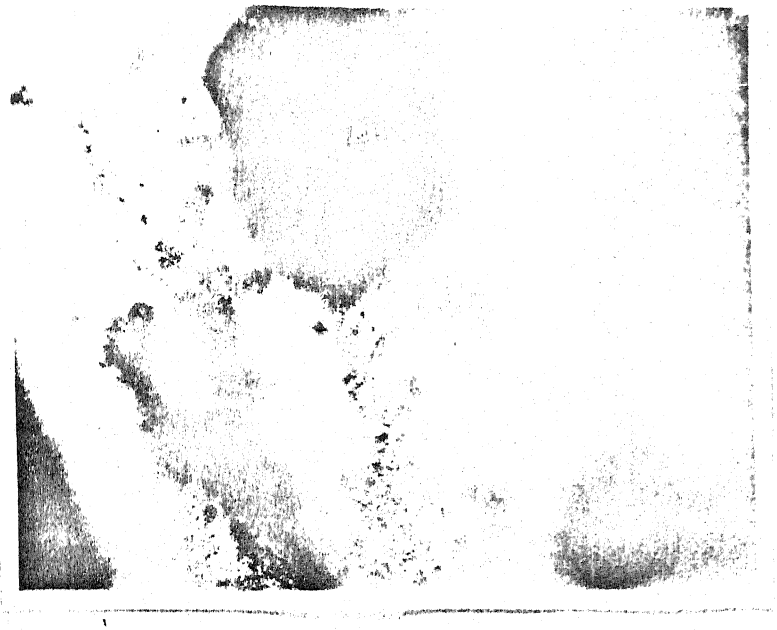

Fig.2.1 : Shows the Locked Particle at -35+48 mesh Size Particles

Fig.2.2 : Shows the Locked Quartz Particle in the Matrix

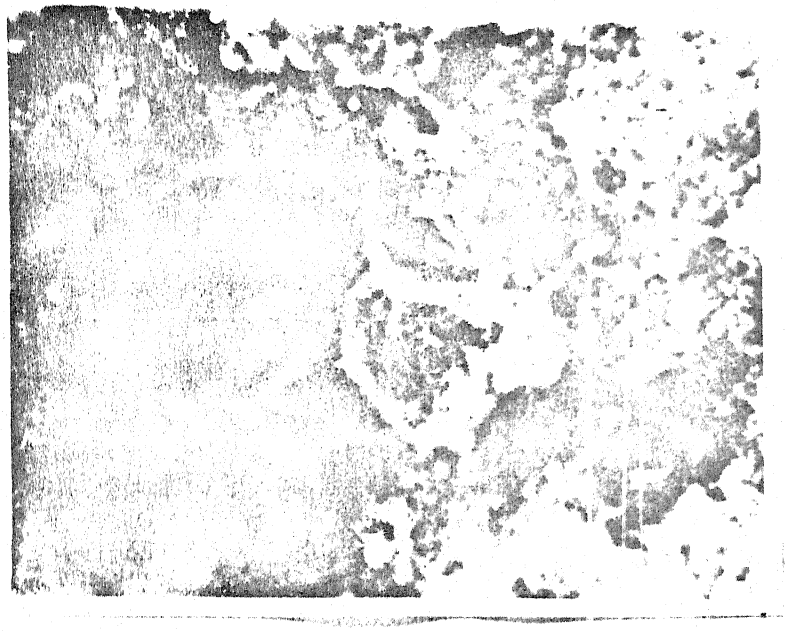

Fig.2.3 : Shows a Smallest Black Particle Locked in the Matrix

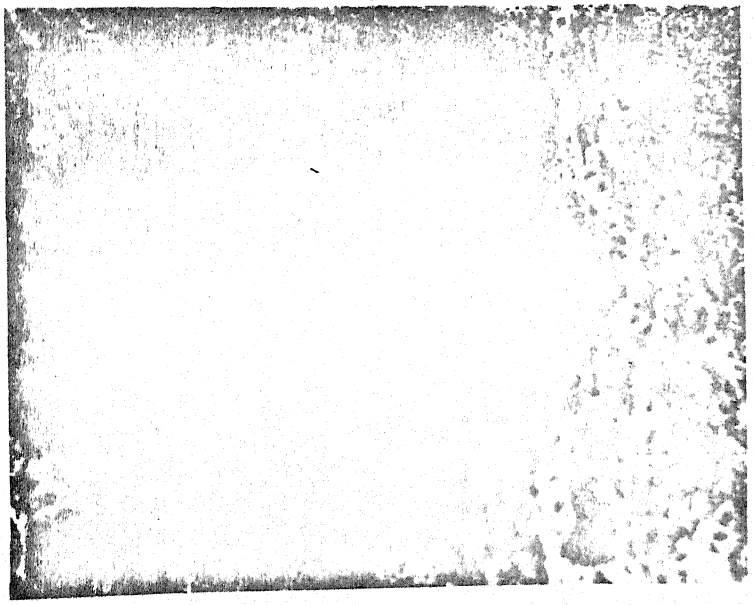

Fig.2.4 : Shows the Presence of Black Particle along the Grain Boundary

Fig.2.5 : Shows Separate Quartz and Magnetite Particle Locked in Hematite Matrix

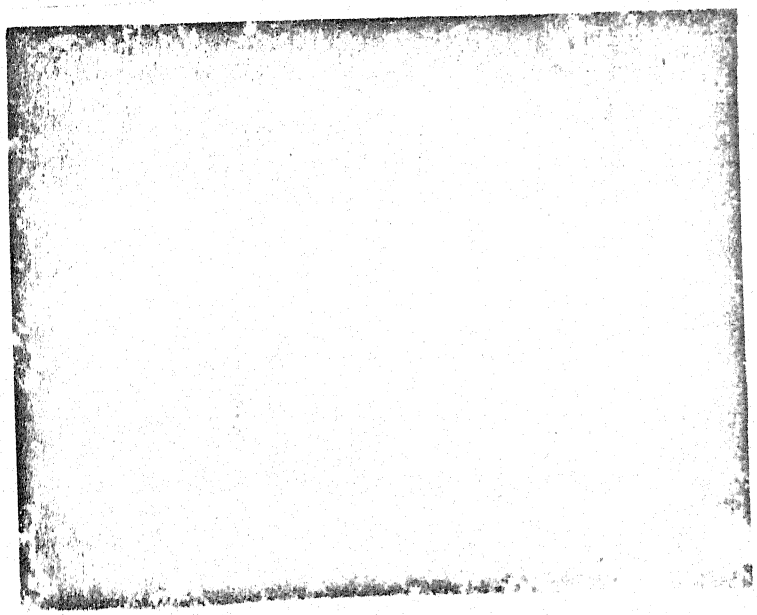

Fig.2.6 : Shows the Presence of Some Red Phase along the Grain Boundary of Quartz

Fig.2.7 : Gives Grain Size Information of Brown Particle

Fig.2.8 : Gives Grain Size Information of Red Particle

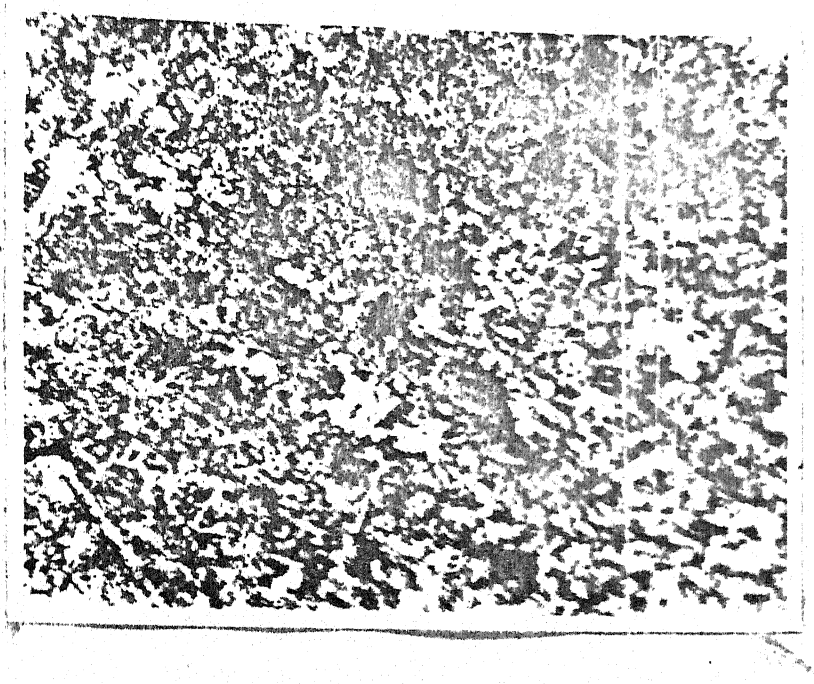

Fig.2.9 : Microstructure of Black Particle

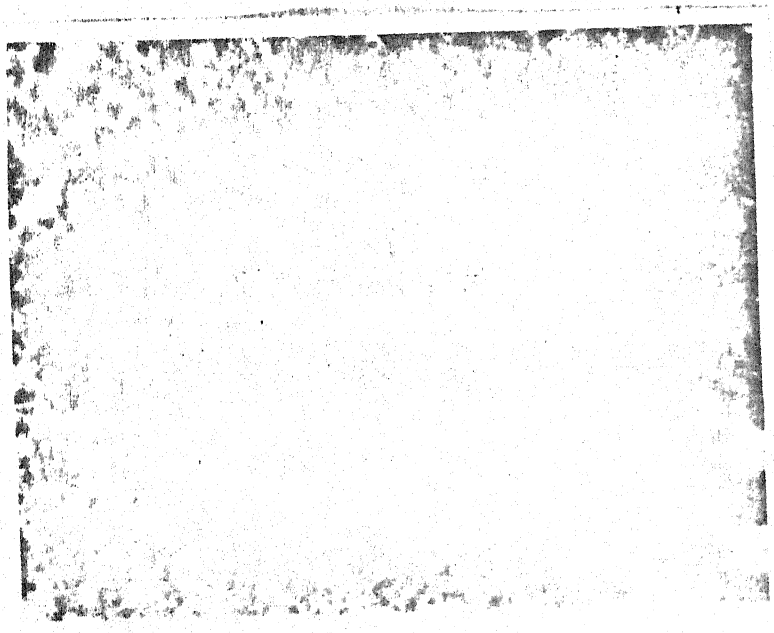

Fig.2.10 : Microstructure of Brown Particle

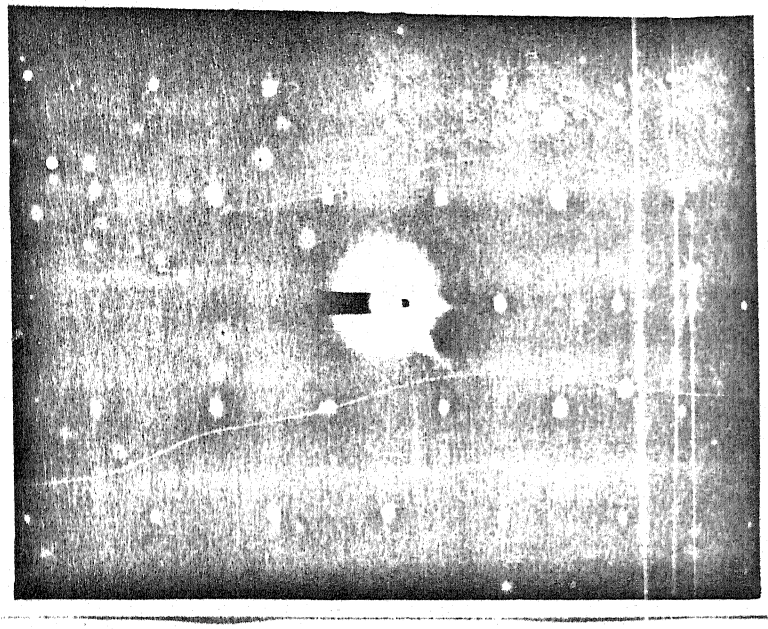

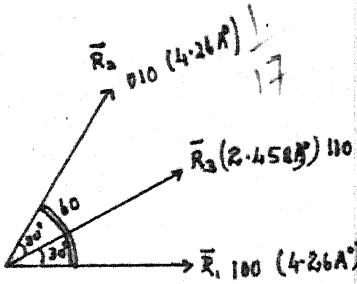

Fig-4.1 S.A.D. of 4.2

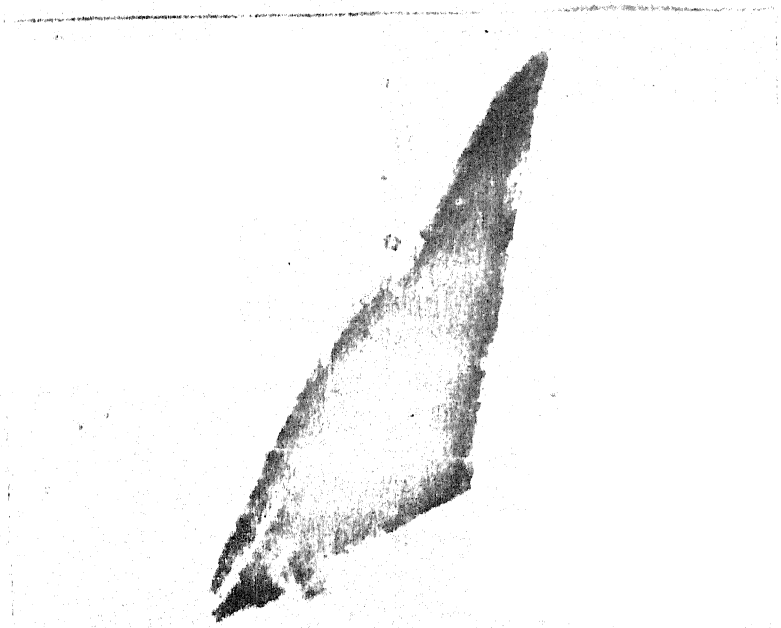

Fig-4.2 Micrograph of the particle taken at magn fication = x

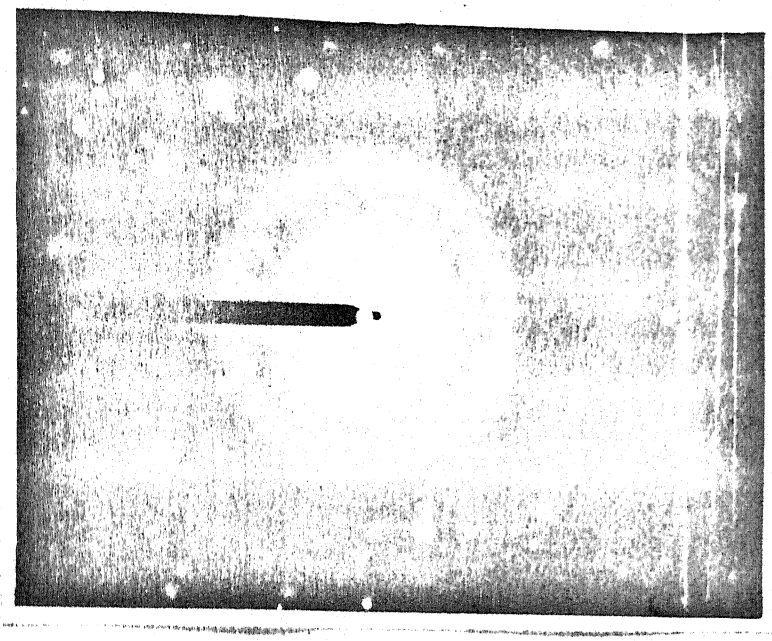

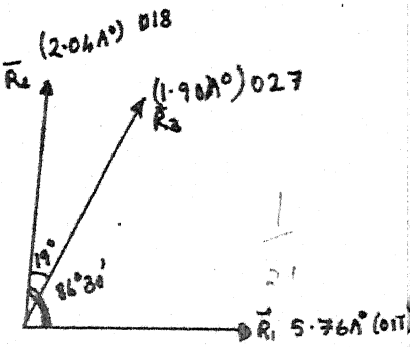

Fig-4·3 S.A.D. of 4.4

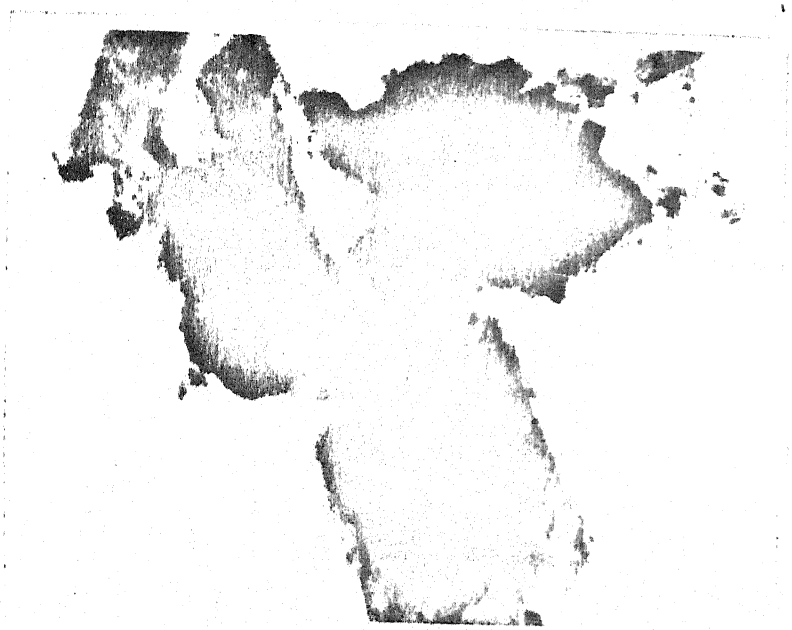

Fig-4·4 Micrograph of the particle taken at magn fication = x

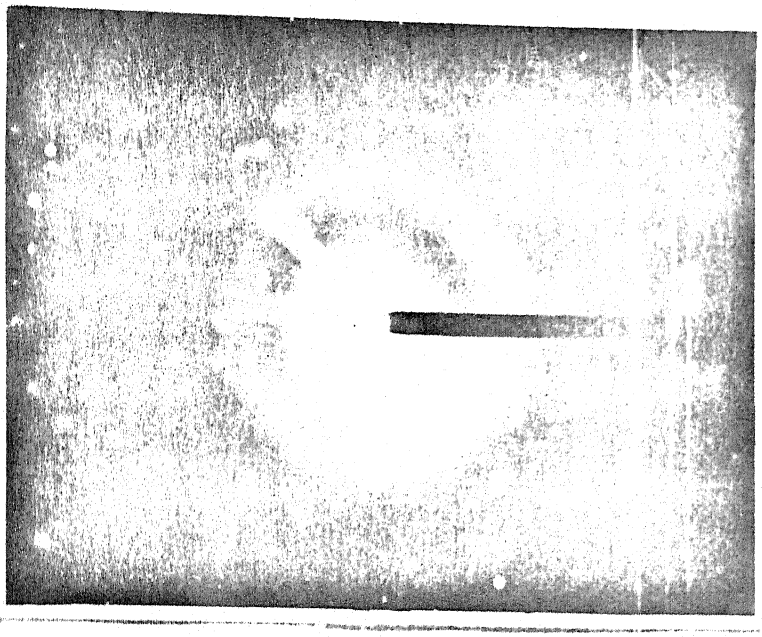

Fig-4·5 S.A.D. of 4.6

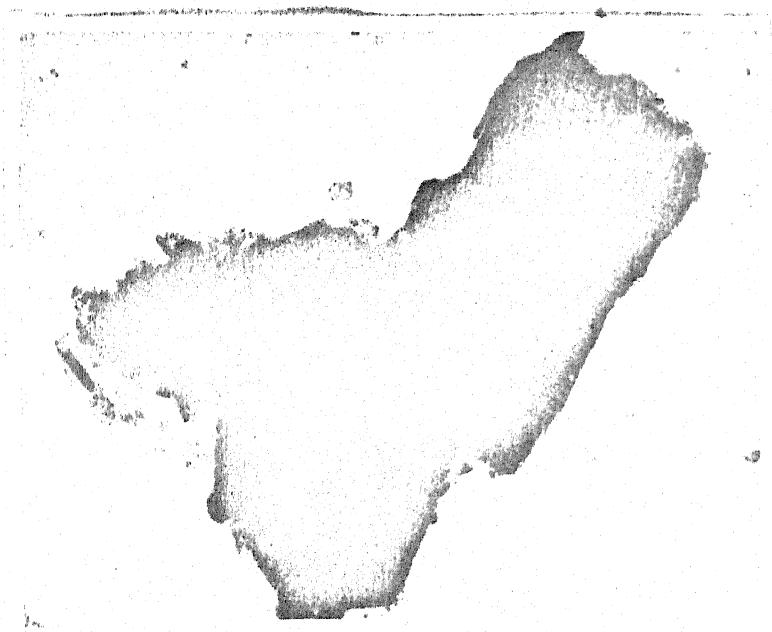

Fig-4·6 Micrograph of the particle taken at magn fication = x

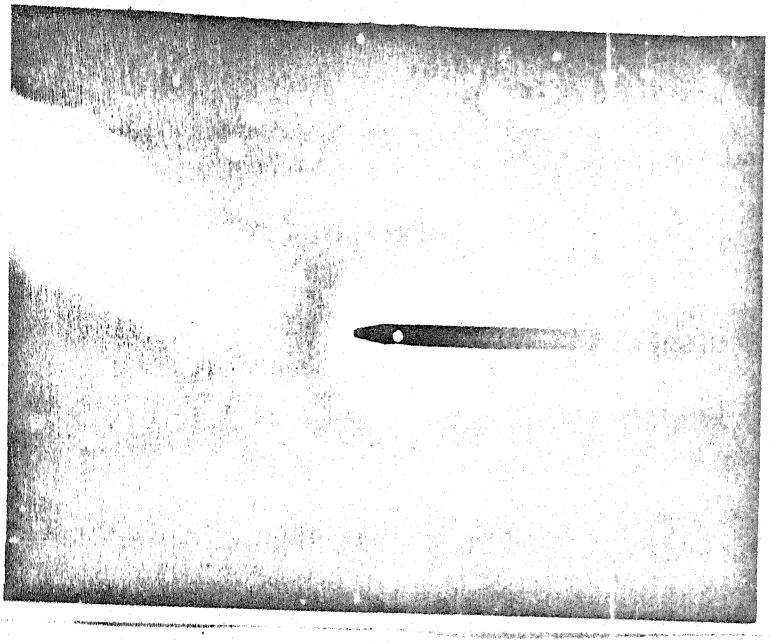

Fig-4·7 S.A.D. of 4.8

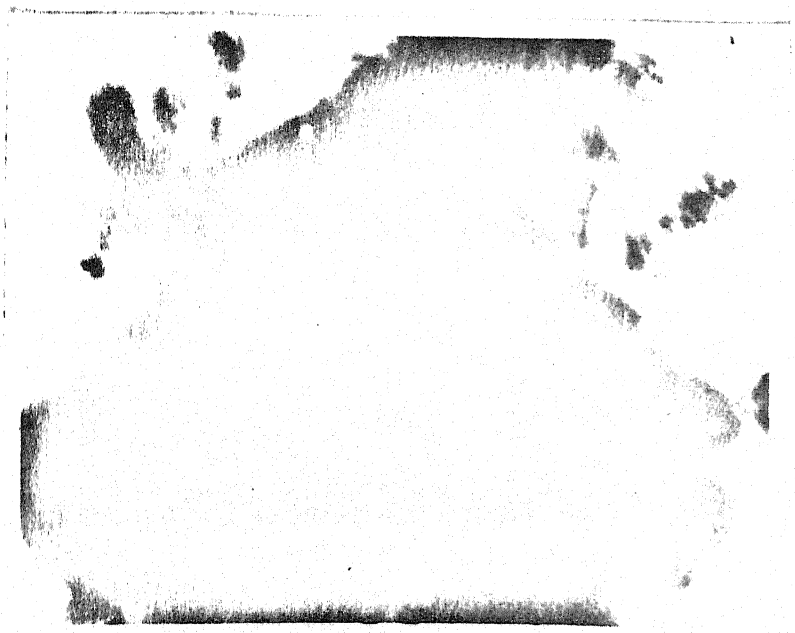

Fig-4·8 Micrograph of the particle taken at magn fication = x

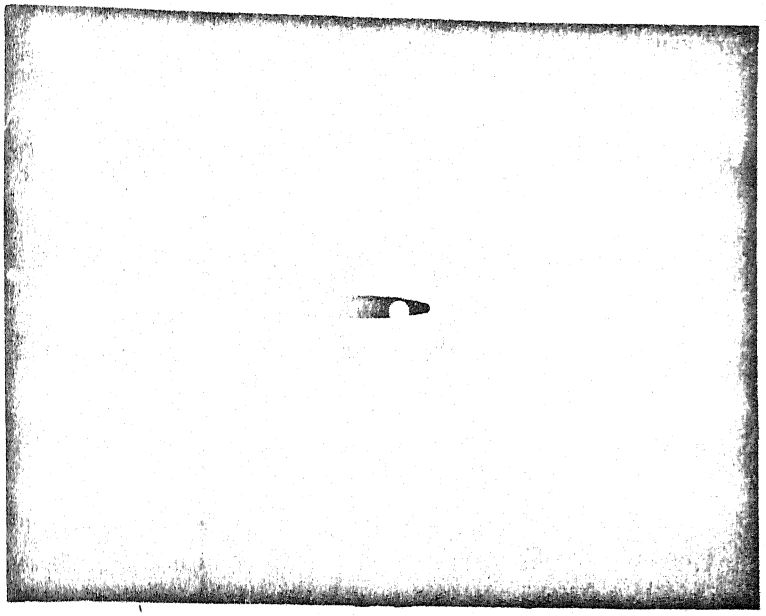

Fig- 4.9 S.A.D. of 4.10

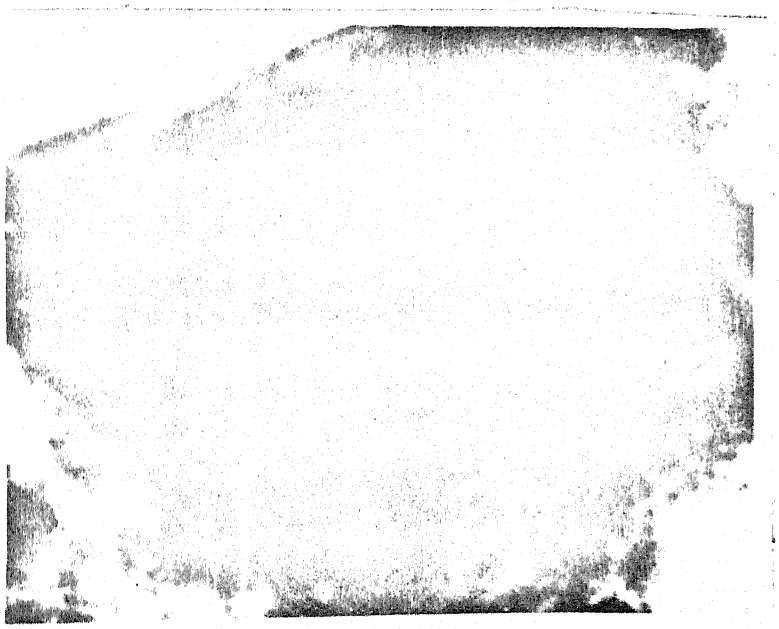

Fig- 4.10 Micrograph of the particle taken at magn fication = x

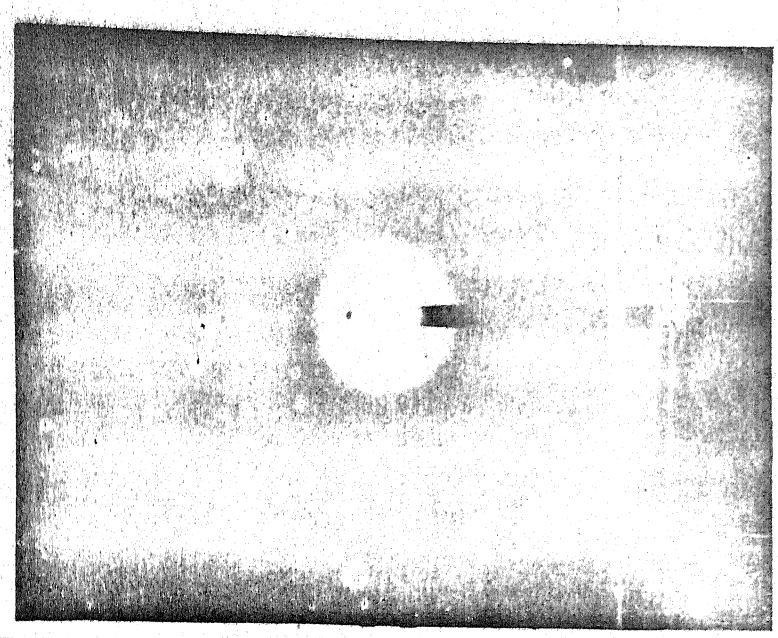

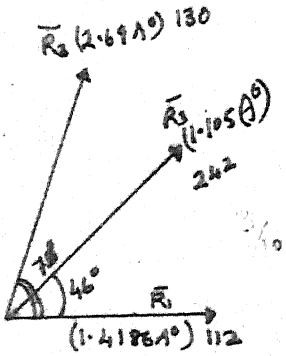

Fig. 4·11 S.A.D. of 4.12

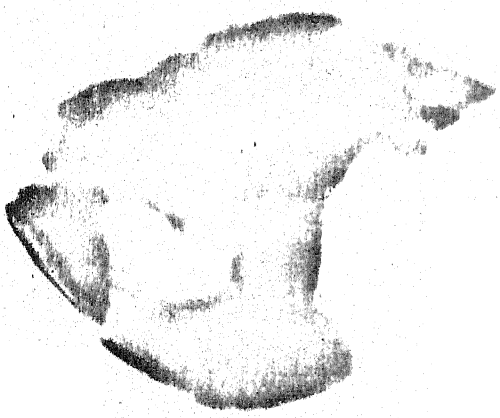

Fig. 4·12 Micrograph of the particle taken at magn fication = x

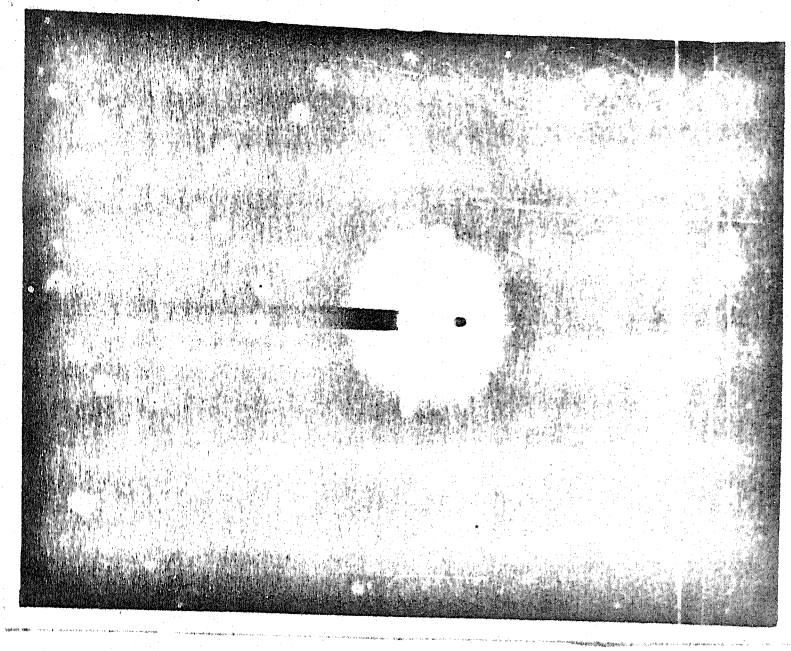

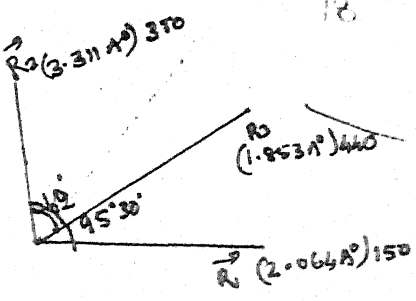

Fig-4.13 S.A.D. of 4.14

Fig-4.14. Micrograph of the particle taken at magn fication = x

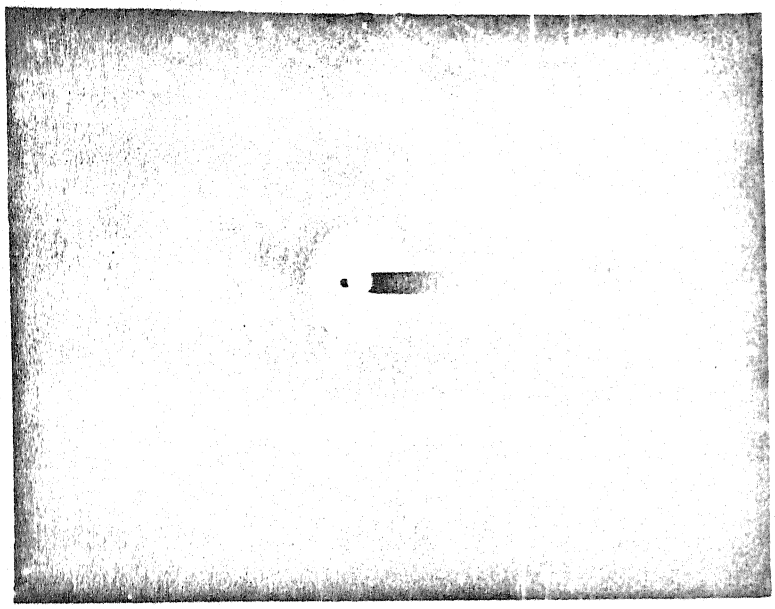

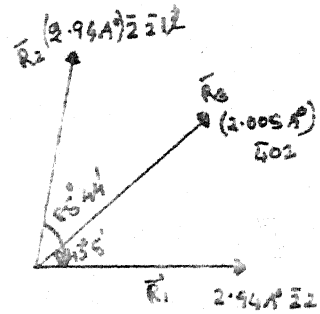

Fig-4.15 S.A.D. of 4.16

Fig. 4.16 Micrograph of the particle taken

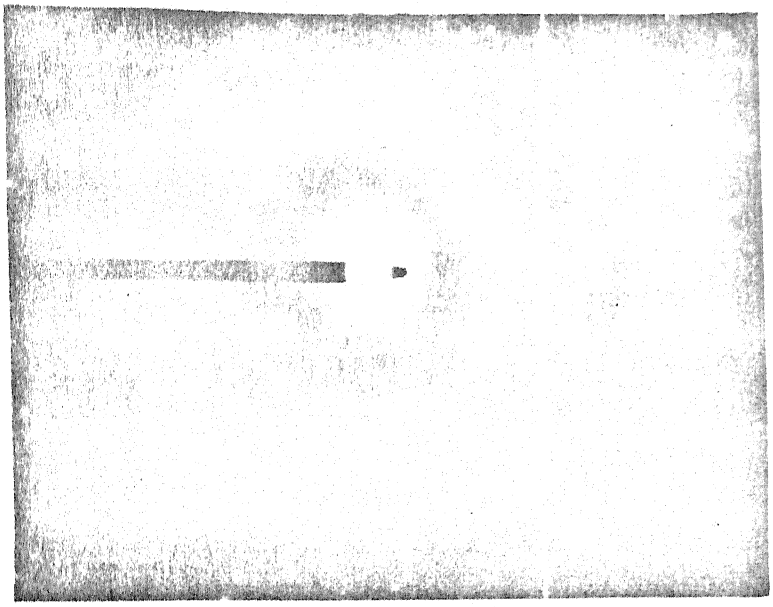

Fig-4.17 S.A.D. of 4.18

Fig-4.18 Micrograph of the
at magn fication

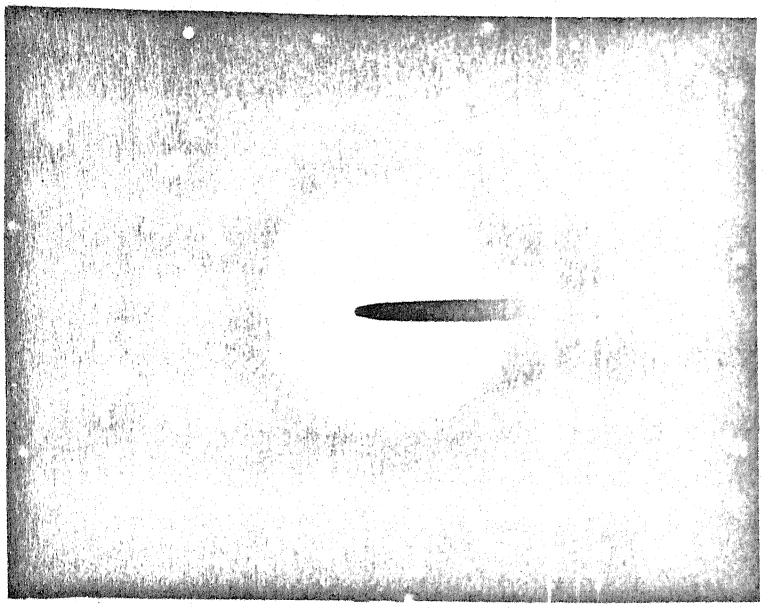

Fig-4.19 S.A.D. of 4.20

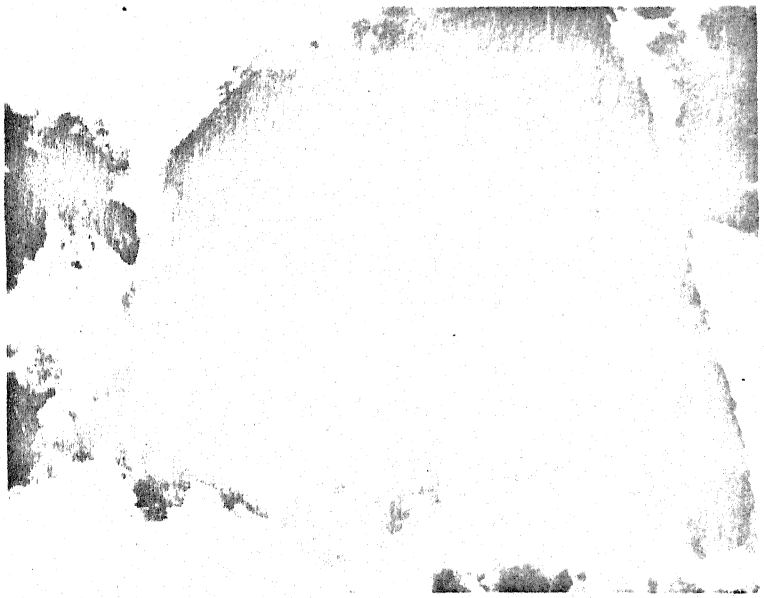

Fig 4.20 Micrograph of the particle taken at magn fication = x

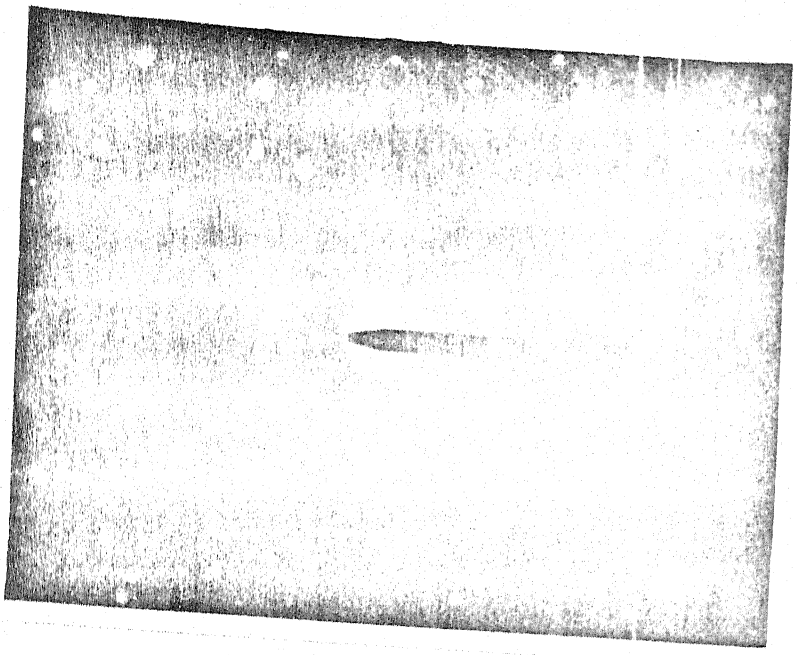

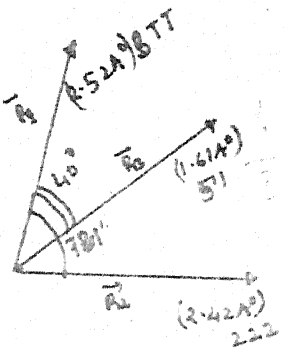

Fig- 4.21 S.A.D. of 4.22

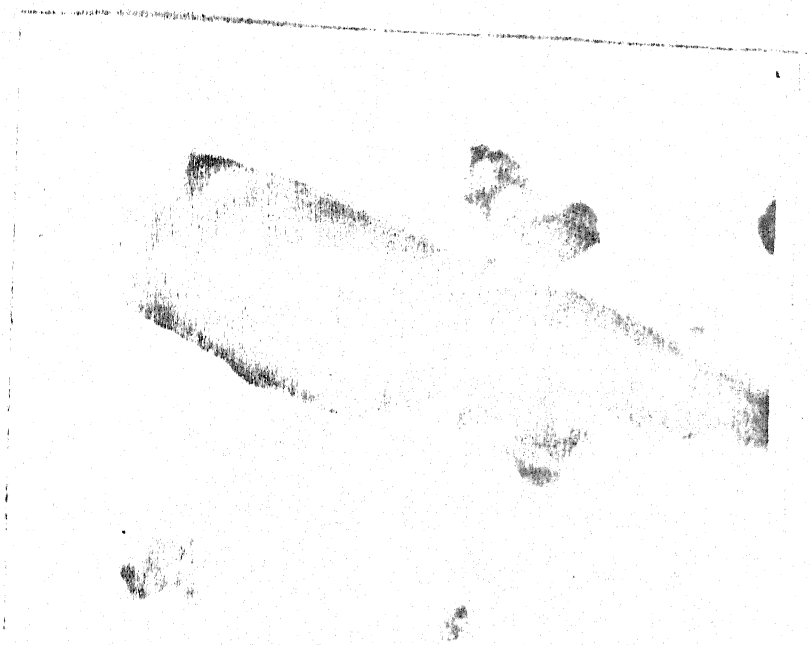

Fig-4.22 Micrograph of the particle taken at magn fication = x